



Transcriptional profiling of *C. elegans* DAF-19 uncovers a ciliary base-associated protein and a CDK/CCRK/LF2p-related kinase required for intraflagellar transport

Prasad Phirke^a, Evgeni Efimenko^{a,1,2}, Swetha Mohan^{b,1}, Jan Burghoorn^{a,3}, Filip Crona^{a,4}, Mathieu W. Bakhom^b, Maria Trieb^{a,5}, Kim Schuske^c, Erik M. Jorgensen^c, Brian P. Piasecki^a, Michel R. Leroux^{b,*}, Peter Swoboda^{a,**}

^a Karolinska Institute, Center for Biosciences at NOVUM, Department of Biosciences and Nutrition, S-141 83 Huddinge, Sweden

^b Simon Fraser University, Department of Molecular Biology and Biochemistry, Burnaby, British Columbia V5A 1S6, Canada

^c University of Utah, Department of Biology and Howard Hughes Medical Institute, Salt Lake City, UT 84112-0840, USA

ARTICLE INFO

Article history:

Received for publication 21 January 2011

Revised 19 June 2011

Accepted 20 June 2011

Available online 27 June 2011

ABSTRACT

Cilia are ubiquitous cell surface projections that mediate various sensory- and motility-based processes and are implicated in a growing number of multi-organ genetic disorders termed ciliopathies. To identify new components required for cilium biogenesis and function, we sought to further define and validate the transcriptional targets of DAF-19, the ciliogenic *C. elegans* RFX transcription factor. Transcriptional profiling of *daf-19* mutants (which do not form cilia) and wild-type animals was performed using embryos staged to when the cell types developing cilia in the worm, the ciliated sensory neurons (CSNs), still differentiate. Comparisons between the two populations revealed 881 differentially regulated genes with greater than a 1.5-fold increase or decrease in expression. A subset of these was confirmed by quantitative RT-PCR. Transgenic worms expressing transcriptional GFP fusions revealed CSN-specific expression patterns for 11 of 14 candidate genes. We show that two uncharacterized candidate genes, termed *dyf-17* and *dyf-18* because their corresponding mutants display dye-filling (*Dyf*) defects, are important for ciliogenesis. DYF-17 localizes at the base of cilia and is specifically required for building the distal segment of sensory cilia. DYF-18 is an evolutionarily conserved CDK7/CCRK/LF2p-related serine/threonine kinase that is necessary for the proper function of intraflagellar transport, a process critical for cilium biogenesis. Together, our microarray study identifies targets of the evolutionarily conserved RFX transcription factor, DAF-19, providing a rich dataset from which to uncover—in addition to DYF-17 and DYF-18—cellular components important for cilium formation and function.

© 2011 Elsevier Inc. All rights reserved.

Introduction

Cilia and flagella are homologous cellular structures used for various sensory and motility-based functions in most eukaryotic cells (Davis et al., 2006; Marshall and Nonaka, 2006). At the core of a cilium

is an axoneme, a microtubule-based structure that is templated by a modified centriole termed basal body. Cilia are complex subcellular organelles that are composed of over 300 proteins (Inglis et al., 2006; Pazour et al., 2005). The formation and maintenance of cilia relies on a bidirectional transport process, termed intraflagellar transport (IFT), which facilitates the movement of proteins within the organelle (Rosenbaum and Witman, 2002). During IFT, ciliary components move between the basal body, which acts as a transport and docking hub, and the distal tip of the cilium, via one or more anterograde kinesin molecular motors (heterotrimeric Kinesin-II and homodimeric OSM-3/KIF17). The IFT machinery and other ciliary components are then recycled back to the base by the action of retrograde cytoplasmic dynein motor 1b (Blacque et al., 2008; Pedersen and Rosenbaum, 2008; Qin et al., 2005; Rosenbaum and Witman, 2002; Scholey, 2008; Silverman and Leroux, 2009). Associated with the IFT motors are two multi-protein subcomplexes (A and B) and a BBS protein complex that are thought to function in the trafficking of specific ciliary cargo, including structural and signaling components required for the specification of different types of cilia (Blacque et al., 2008; Pedersen and Rosenbaum, 2008; Rosenbaum and Witman, 2002; Silverman and Leroux, 2009).

* Correspondence to: M. R. Leroux, Simon Fraser University, Department of Molecular Biology and Biochemistry, Burnaby, British Columbia V5A 1S6, Canada.

** Correspondence to: P. Swoboda, Karolinska Institute, Center for Biosciences at NOVUM, Department of Biosciences and Nutrition, Hälsovägen 7, S-141 83 Huddinge, Sweden. Fax: +46 8 774 5538.

E-mail addresses: leroux@sfu.ca (M.R. Leroux), peter.swoboda@ki.se (P. Swoboda).

¹ EE and SM contributed equally and should be regarded as joint second authors.

² Present address: Dartmouth Medical School, Department of Genetics, 7400 Rensselaer, Hanover, NH 03755, USA.

³ Present address: Bonsema Bouw B.V., Hoofdweg 38, NL-9945 Wagenborgen, The Netherlands.

⁴ Present address: Stockholm University, Wenner-Gren Institute for Developmental Biology, S-106 91 Stockholm, Sweden.

⁵ Present address: Medical University Innsbruck, Department of Medical Genetics, Molecular and Clinical Pharmacology, Division of Biochemical Pharmacology, A-6020 Innsbruck, Austria.

In humans, cilia are required for the development and homeostasis of most cells, tissues, and organs. For example, nodal cilia concentrate growth factors to one side of the developing embryo, resulting in the left-right asymmetric patterning of organs (Tabin and Vogan, 2003). Respiratory cilia in the mammalian lung sense noxious substances and propel mucus across the epithelial lining (Shah et al., 2009). Highly specialized cilia in photoreceptor cells concentrate the membrane-bound phototransduction machinery (Wolfrum and Schmitt, 2000). Primary cilia play critical roles in several signal transduction pathways, including Sonic hedgehog (Moussaif and Sze, 2009; Wong et al., 2009), platelet-derived growth factor receptor- α (Christensen et al., 2008), Wnt, and cyclic nucleotide signaling (Johnson and Leroux, 2010; Lancaster et al., 2009).

Human ciliopathies are a class of genetic disorders that can be attributed to defects in cilia-related functions. Examples of these disorders include the multi-systemic Bardet–Biedl and Meckel syndromes (Zaghloul and Katsanis, 2009), Polycystic Kidney Diseases (Haycraft et al., 2001), retinal degenerative diseases (Adams et al., 2007), and reproductive dysfunction (Rashid et al., 2010). In vertebrates, disruption of IFT proteins causes embryonic lethality and ciliopathy-associated proteins are often critical for early development, making it difficult to study some cilia-related proteins or processes (Cortellino et al., 2009; Howard et al., 2010).

The worm *Caenorhabditis elegans* provides a relatively simple animal model system for studying ciliary genes, including orthologues of numerous ciliopathy genes (Bialas et al., 2009; Blacque et al., 2004; Cevik et al., 2010; Jauregui et al., 2008; Li et al., 2010; Williams et al., 2008; Williams et al., 2010; Winkelbauer et al., 2005). *C. elegans* cilia are exclusively found extending from the distal dendritic processes of a subset of terminally differentiated sensory neurons, the so-called ciliated sensory neurons (CSNs). Many CSNs facilitate sensory input from the external environment. In the *C. elegans* nervous system, 61 of the 302 neurons found in an adult hermaphrodite animal are ciliated (Perkins et al., 1986; Ward et al., 1975) (www.wormatlas.org). The best-characterized *C. elegans* cilia are the amphid (head) and phasmid (tail) cilia, which consist of a basal body, a transition zone region as well as middle and distal ciliary segments. The nematode basal body degenerates during development, so that only the transition fibers, structures found at the distal end of all basal bodies, are clearly observed (Perkins et al., 1986). The transition zone, which is positioned immediately adjacent to the basal body, is structurally identical to those found in other ciliated organisms, with characteristic Y-links that join the axoneme to the ciliary membrane. The middle and distal ciliary segments of *C. elegans* cilia are distinguishable by the presence of an array of 9 doublet followed by 9 singlet microtubules, respectively.

Ciliary development in *C. elegans* is controlled by DAF-19, the sole RFX transcription factor in this organism (Swoboda et al., 2000). This transcription factor is conserved in many eukaryotes and has been shown to also be important for regulating ciliary gene expression in *Drosophila* and mammals (Baas et al., 2006; Chu et al., 2010; El Zein et al., 2009; Laurencon et al., 2007; Piasecki et al., 2010). The initial expression of DAF-19 coincides with the development of most CSNs during embryogenesis (Senti and Swoboda, 2008). A null mutation in DAF-19 leads to a complete loss of cilia (Perkins et al., 1986; Swoboda et al., 2000). Importantly, *daf-19* mutant worms are viable but are unable to respond to various sensory stimuli and have developmental defects, such as constitutive entry into the dauer (stress-resistant) larval stage (Perkins et al., 1986; Swoboda et al., 2000). Thus, the *C. elegans daf-19* mutant provides a powerful genetic system for identifying novel target ciliary genes, and is particularly advantageous compared to vertebrate or mammalian species for studying genes that may have essential functions.

Several genome-wide approaches have revealed numerous genes involved in ciliogenesis and ciliary maintenance in *C. elegans*. Detailed analyses, which include studies conducted in other organisms, were

previously presented (Arnaiz et al., 2009; Gherman et al., 2006; Inglis et al., 2006). Novel ciliary genes were identified by conducting genome-wide searches for X-box promoter motifs, the binding sites of DAF-19 (Blacque et al., 2005; Chen et al., 2006; Efimenko et al., 2005). This approach has been complemented by microarray analyses of non-synchronized *daf-19* mutant and wild-type embryos to identify genes directly and indirectly regulated by the DAF-19 RFX transcription factor (Chen et al., 2006). Another approach used serial analysis of gene expression (SAGE) to uncover novel subsets of genes enriched in CSNs (Blacque et al., 2005). Similarly, CSN mRNAs were isolated using a poly-A tail pull-down approach (Kunitomo et al., 2005). Lastly, genes of specific sensory neuron types were selectively identified by microarray analysis of RNA from sorted AWB olfactory and AFD thermosensory neurons (Colosimo et al., 2004). Although these approaches have identified many genes associated with the development of cilia, genes that function in this process very likely remain to be identified.

To identify genes that might be specifically involved in the development of cilia we have focused on RNAs expressed during the narrow time period in which CSNs are born and differentiate. We compare microarray expression profiles of *daf-19* mutant and wild-type worms using RNA from embryos staged to a time coinciding with the development of cilia and the differentiation of CSNs. To validate the data obtained from our microarray profiles, we conducted both quantitative RT-PCR and anatomical expression pattern analyses on select candidate genes from our microarray studies. From these studies, two candidate genes, *dyf-17* and *dyf-18*, were selected for further functional characterization. DYF-17, highly conserved among *Caenorhabditis* species, was found to play a role at the base of cilia, where it influences the formation of the distal ciliary segment. DYF-18, an evolutionarily conserved CDK7/CCRK/LF2p-type serine/threonine kinase, was demonstrated to influence the behavior of IFT proteins and shown to be required for ciliogenesis. Collectively, our findings identify a list of temporally-defined DAF-19 transcription factor targets. In addition to uncovering two novel genes required for ciliogenesis (*dyf-17* and *dyf-18*) our dataset will be useful for the discovery and characterization of novel genes implicated in ciliogenesis and ciliary functions.

Materials and methods

C. elegans worm strains and culture conditions

All *C. elegans* strains used in this study were grown and cultured at 20 °C following standard procedures (Brenner, 1974), are described in Supplemental Table 1. Because *daf-19* (*m86*) mutants display a highly penetrant dauer constitutive (Daf-c) phenotype at all temperatures, a *daf-12* (*sa204*) mutation was introduced into the genetic background of all *daf-19* strains used in this study. While the *daf-12* mutation fully suppresses the Daf-c phenotype of *daf-19*, cilia remain completely absent in *daf-19*; *daf-12* double mutants (Senti et al., 2009).

Dye-filling and osmotic avoidance assays

Fluorescent dye-filling assays were performed essentially as described (Starich et al., 1995) using the fluorescent dye Dil (Molecular Probes; DiI₁₈ Vybrant Dil cell-labelling solution, diluted 1:1000 with M9 buffer). Adult hermaphrodites were stained, and Dil uptake into the amphid and phasmid neurons was visualized using conventional fluorescence microscopy (Zeiss Axioplan 2 or Axioskop 2+; Carl Zeiss AG, Göttingen, Germany) using a Texas Red filter. Fluorescence intensities of Dil were quantified using ImageJ. The fluorescent dye-filling defective (Dyf) mutant strains CB3323 *che-13* (*e1805*) and PR813 *osm-5* (*p813*) were used as controls for the Dyf phenotype. Osmotic avoidance assays were performed essentially as described (Culotti and Russell, 1978) by testing the ability of adult hermaphrodite worms to cross a ring of high osmotic strength (8 M glycerol). The osmotic

avoidance defective (*Osm*) *che-13* and *osm-5* mutants were used as controls.

Genetic characterization of the *dyf-17* and *dyf-18* mutants

The original mutant strain EG175 *dyf-17* (*ox175*) was outcrossed to generate the *ox175* homozygous mutant strains OE3663 (2× outcrossed) and OE4013 (4× outcrossed). No phenotypic differences were observed when comparing between 2× and 4× outcrossed strains. For *dyf-17* rescue experiments, the *dyf-17* promoter and gene-coding regions were amplified by PCR from worm genomic DNA. The OE3663 and OE4013 strains were used for germline transformations of this DNA as described (Mello et al., 1991). The original mutant strain ET100 *dyf-18* (*ok200*) was outcrossed six times before rescue and phenotypic characterization experiments.

Preparation of ciliary gene transcriptional and translational fusion constructs

Transcriptional GFP reporter constructs were generated using fusion-PCR (Hobert, 2002). Typically, 2 Kb promoter regions from genes of interest were individually fused in-frame to the GFP coding sequence amplified from the plasmid pPD95.75 using PCR. A *dyf-17* translational GFP construct was generated by fusing the same GFP coding sequence to the entire gene-coding region of *dyf-17* and its corresponding 2 Kb promoter. Germline transformations were conducted for all transcriptional and translational GFP fusions using microinjection (Mello et al., 1991). Gel purified PCR products were injected at 100 ng/μl for transcriptional GFP fusions and a variety of concentrations, as indicated, for translational GFP fusions. An *elt-2p::mCherry* co-transformation marker (a gift from Gert Jansen) was used at 20 ng/μl in addition to all transgenes. Worms expressing mCherry in the intestine were selected as being transgenic and then analyzed for GFP expression by standard microscopy procedures. To create a DYF-18::gfp translational fusion construct, the entire coding region, including 642 bp of promoter, was fused to a DNA fragment containing GFP and the *unc-54* 3' UTR (amplified from the GFP expression vector pPD95.77). Transgenic lines carrying the DYF-18::gfp translational GFP construct were generated by microinjection into the strain MX41 *dpy-5* (*e907*); *Ex* [*dpy-5*(+)] and maintained as extrachromosomal arrays. For transgenic rescue of *dyf-18*, 50 ng/μl of the DYF-18::gfp translational GFP construct were injected into the strain ET100 *dyf-18* (*ok200*) along with *dpy-30::dsRed* as a co-injection marker.

Microscopy and imaging

GFP expression patterns were analyzed in stable transgenic lines using conventional fluorescence microscopy (Zeiss Axioplan 2 or Axioskop 2+) and confocal microscopy (Zeiss LSM510 META). Expression patterns were examined in at least two independent transgenic lines for most developmental stages. For visualization of GFP-tagged intraflagellar transport proteins, worms were immobilized using 15 mM levamisole, mounted on 2% agarose pads and examined on a WaveFX spinning disc confocal system (Quorum Technologies) using a 100×, 1.40NA objective. Images were acquired using OpenLab software (Improvision, Coventry, United Kingdom). Quantitation of Dil uptake was performed using ImageJ. Determination of neuronal cell identities followed published descriptions (Ward et al., 1975).

daf-19 microarray expression profiling

Embryo preparation for microarray and quantitative real-time PCR

Embryos were harvested from JT204 *daf-12* (*sa204*) and JT6924 *daf-19* (*m86*); *daf-12* (*sa204*) mutants. Worms were grown on agarose containing solid egg-NGM medium for 6–7 days until a sizeable gravid adult worm population was observed. Embryos were then isolated from

gravid adults by hypochlorite treatment, a procedure that kills and removes all larval and adult worms. The resulting population of mixed-staged embryos was pelleted and suspended in 15–20 ml of S-Basal medium. Embryos in this solution were placed on a gently rotating orbital shaker at 20 °C for approximately 8 h, until the majority of embryos had developed into 3-fold stage embryos. A second hypochlorite treatment removed any hatched worms or dead eggs and left an egg sample selectively enriched for 3-fold stage embryos. Quantification of this approach demonstrated that approximately 90–95% of the remaining worm population was at the 3-fold stage of embryogenesis. Worm embryos obtained using these methods were immediately frozen in 0.5 to 1 ml of Trizol solution (Invitrogen Inc. San Diego, CA, USA) and stored at –70 °C prior to being used for total RNA extraction.

RNA extraction, analysis, cDNA preparation and labeling

Harvested worm embryos were passed through three sequential freeze and thaw cycles using liquid nitrogen and a 37 °C water bath. The resulting mixture was then crushed using a dounce homogenizer and total RNA was isolated using a standard phenol-chloroform extraction procedure. The resulting pellet was suspended in nuclease-free water (Ambion Inc., Foster City, CA, USA), and the quantity and quality of the extracted RNA was determined using a Nanodrop (Thermo Scientific Inc, Wilmington, DE, USA) and Agilent Bioanalyzer 2100 (Agilent Inc, Santa Clara, CA, USA), respectively. All RNA samples obtained in sufficient concentration and quality were used for subsequent microarray hybridizations. A standard eukaryotic target preparation protocol using 5 μg of total RNA was conducted for each array as described in the Affymetrix GeneChip Eukaryotic Sample labeling protocol. (Affymetrix Inc.). A total of four independent array hybridizations from each strain were performed as described in the GeneChip Expression Analysis technical manual (Affymetrix Inc.). In-vitro transcription, fragmentation, hybridization, staining and scanning were performed by the Bioinformatics and Expression Analysis core facility at NOVUM, Karolinska Institute, Stockholm-Huddinge, Sweden (www.bea.ki.se).

Raw data generation

Subsequent to scanning, arrays were subjected to a range of low stringency analyses, including image analyses, signal summarization, and normalization. The expression reports were then examined to confirm that the values of all internal controls were within the acceptable range, as defined by the Affymetrix Data Analysis Fundamentals (Affymetrix, Inc). Data that passed all quality control measures was then utilized for further statistical analyses. This microarray dataset has been submitted to the Gene Expression Omnibus (GEO) database (Barrett and Edgar, 2006). The GEO accession number is GSE25633.

Statistical data analysis

The CEL files obtained from array hybridizations were imported into RMAExpress (version 0.3) (<http://rmaexpress.bmbolstad.com>) and the expression signal values were calculated using a robust multichip average (RMA) expression summary and quantile normalization technique. This normalization technique considers only perfect match probes when calculating signal values and consequently excludes the use of mismatch probes, such as those used by the GeneChip® operating software (GCOS; Affymetrix, Inc). BRB Array Tools (version 3.3; <http://linus.nci.nih.gov/BRB-ArrayTools.html>) was subsequently used to identify genes with a statistically significant variation in expression when comparing between the two classes defined in this study. The probability threshold was set at a maximum of 0.05 ($p\text{-value} \leq 0.05$) for genes to be considered statistically different. Genes with a signal variation of 1.5-fold or greater were selectively identified for use in all subsequent experiments. To reduce the chances of false discoveries, a class comparison test was conducted using a multivariate permutation test with the confidence level of 97%. This permutation is very similar to the one utilized in the

Significance Analysis of Microarrays (SAM) analyses (Tusher et al., 2001). Additional lists of genes were generated using SAM (version 2.2) with a false discovery rate (FDR) of less than or equal to 5% ($Q\text{-value} \leq 5\%$). Twenty-seven repeated runs of SAM were performed using variable random seed numbers for each run. During each run of SAM, 100 permutations were performed. Genes ($n = 129$ downregulated, $n = 1$ upregulated) appearing in at least 80% of all twenty-seven runs of SAM were further considered for signal variation filtering, which was used to selectively identify genes with a 1.5-fold or greater variation between the two genetic conditions used for comparison.

Quantitative real-time PCR (RT-PCR) analysis

A total of 10 μg from each total RNA sample was subjected to DNase digestion (TURBO DNase-free reagents, Ambion) and single-strand cDNA synthesis (iScript; Bio-Rad, Sweden) according to the manufacturer's protocol. Samples were confirmed for quantity and quality using both Nanodrop and Agilent Bioanalyzer 2100. Out of each 100 μl reaction mix, 4 μl were subsequently used for RT-PCR. The cDNA was analyzed in a MyiQ thermal cycler (BioRad Laboratories, Sweden). Amplification efficiencies for each primer pair were calculated as a mean of all samples using LinReg PCR (Ramakers et al., 2003). The resulting C_t -values were then converted into raw quantities, including the amplification efficiencies, using the ΔC_t method as described in the Genorm manual (Vandesompele et al., 2002). Raw gene quantities were used to calculate the geometric mean of the two reference genes, which were used as normalization factors for each cDNA sample. The stability measure M (Vandesompele et al., 2002) for the mean of the housekeeping genes *gpn-1* and *ppp-1* was below 1.5 for the two mutant conditions used (JT204 versus JT6924). Normalized expression levels were calculated by dividing the raw quantities of the genes of interest for each sample by the corresponding normalization factors. Outliers were detected and removed from the dataset using a Grubb's test (<http://www.graphpad.com/quickcalcs/Grubbs1.cfm>).

Results

Identification of new candidate ciliary genes

To identify ciliary genes that are directly and indirectly regulated by the *C. elegans* RFX transcription factor DAF-19, hybridizations were conducted on Affymetrix whole-genome microarrays. RNA was isolated from worms synchronized to a developmental stage when ciliogenesis occurs in most ciliated sensory neurons (CSNs). The expression profiles of *daf-19* mutant (JT6924) versus *daf-19* wild-type (JT204) worm populations from four independent biological replicates of highly synchronized 3-fold stage worm embryos were compared (Supplemental Fig. 1) (worm strains: Supplemental Table 1). Candidate *daf-19* regulated genes with a statistically significant signal variation of 1.5-fold or greater were subsequently identified using a class comparisons tool from BRB Array Tools and a Significance Analysis of Microarrays (SAM). The class comparisons tool revealed a set of 1433 differentially expressed probe sets with a probability threshold of 0.5% ($p \leq 0.05$). These probe sets include 524 downregulated and 357 upregulated genes in the mutant background compared to the wild-type background with a signal variation of 1.5-fold or greater (881 genes in total; Supplemental Table 2). The SAM analysis revealed 236 genes with a false discovery rate threshold of less than or equal to 5% ($q \leq 5$). Of these 236 genes, 129 downregulated genes and only one upregulated gene passed the criteria of reproducibility using 27 bootstrap replicates (Supplemental Table 2). Subsequent analyses revealed that the SAM candidate gene list constitutes a subset of the class comparison gene list.

Gene ontology analyses were performed on all statistically significant candidate genes identified in this study using the Database for Annotation, Visualization and Integrated Discovery (DAVID)

(Dennis et al., 2003) software package. We functionally classified all candidate genes to various cilia-related processes such as cilium biogenesis, cell projection biogenesis, chemosensory behavior and others (Supplemental Fig. 2, Supplemental Table 3 and data not shown). The identified candidate genes fell into large classes, including known ciliary genes, genes encoding protein domains enriched in cilia, and genes encoding novel proteins. For example, several of the candidate genes encode proteins that contain specific domains enriched in ciliary proteins, including B9, TPR, and WD40 domains. Of note, our gene ontology characterization revealed a significant number of candidate genes with completely unknown functions. Thus, in addition to showing that our candidate gene list is enriched for ciliary genes, these analyses also highlight the importance of further characterizing candidate genes with no known roles in cilium formation or function.

To ascertain the quality of data obtained from these microarray analyses, all candidate genes that satisfied our statistical criteria were compared to biological controls, including a set of well-characterized ciliary genes and candidate ciliary gene lists generated from several previous large-scale bioinformatic, genomic and proteomic studies (Table 1). We found that our candidate gene list contains numerous experimentally verified ciliary genes, including genes with X-box promoter motifs, genes involved in IFT, and CSN-specific genes (Table 1). Our candidate genes were also compared to a MultiSage database, which provided the respective expression profile for each gene (McKay et al., 2003). These analyses revealed that our gene list was highly enriched for genes preferentially expressed in CSNs. Cross-comparisons to the ciliary gene lists generated from other large-scale genomic and proteomic studies revealed that a subset of genes identified here overlapped with the genes revealed from these other complementary studies (Table 1, Supplemental Table 2) (Avidor-Reiss et al., 2004; Blacque et al., 2005; Chen et al., 2006; Colosimo et al., 2004; Efimenko et al., 2005; Laurenzen et al., 2007; Li et al., 2004; Pazour et al., 2005). Importantly, however, our dataset contains a large proportion of completely unknown and uncharacterized genes. For example, for more than 50% of the genes from our dataset no known protein domains have been predicted (<http://pfam.sanger.ac.uk/>), nor have RNAi phenotypes been reported or are their anatomical gene expression patterns known (Supplemental Fig. 2 and data not shown). Because our microarray studies were conducted using worms tightly staged to a developmental stage when most CSNs develop cilia, these comparisons likely reveal ciliary genes that are exclusively or more abundantly expressed/repressed during ciliogenesis.

Quantitative real-time PCR (RT-PCR) analysis

We independently verified that candidate genes identified in our microarray analyses are differentially expressed in the *daf-19* mutant compared to its wild-type counterpart using RT-PCR. For these RT-PCR analyses we selected candidate genes with varying levels of microarray signal down-regulation: (i) three unknown and uncharacterized genes, including C42C1.7, E04A4.6, and F28A12.3, (ii) two CSN-expressed genes of unknown function (C33A12.4 and K07C11.10) (Kunitomo et al., 2005) and (iii) the recently studied MKS3/Meckel-Gruber syndrome ciliopathy gene ortholog, *mks-3* (F35D2.4) (Williams et al., 2010). Two well-characterized ciliary genes, *bbs-1* and *che-13*, were selected as positive controls. Two housekeeping genes, *gpn-1* and *ppp-1*, were selected from within our microarray analyses using a statistical approach that reveals genes with the lowest incidence of signal variation in their expression profile (Shulzhenko et al., 2005). The *gpn-1* gene encodes a glypican protein and the *ppp-1* gene encodes the gamma subunit of the translation initiation factor 2B (eIF2B). A total of three independently isolated RNA samples were used for RT-PCR, including two original sample isolates used in microarray hybridizations and an additional sample isolate. All candidate genes analyzed using RT-PCR

Table 1

(A) Gene expression analyses using transcriptional GFP reporter fusions and quantitative real-time PCR analyses of select ciliary candidate genes revealed by microarrays. Genes in rows 1, 2, 5–9, 11–16, and 18 were analyzed by transcriptional GFP reporter fusions (cf. Figs. 1–3). Genes in rows 3–5, 7, 9, and 13 were analyzed by quantitative real-time PCR. The known ciliary genes *che-13* (row 10) and *bbs-1* (row 17) served as internal controls for both types of analyses. The GFP expression properties of twelve of the eighteen genes listed have been tested for DAF-19 dependence, whereby all seven genes that display DAF-19 dependence are expressed in CSNs, three CSN-specific genes display GFP expression that is independent of DAF-19, while two DAF-19 independent genes are not expressed specifically in CSNs. (B) For comparison the same properties as for the ciliary candidate genes (rows 1–18) have been listed for 33 known ciliary genes with strong experimental support (rows 19–51), as compiled in ciliary gene databases (e.g. Arnaiz et al., 2009; Gherman et al., 2006; Inglis et al., 2006).

Sequence	Gene	Fold-change		Expression pattern	Expression properties	Other studies*								Functions/domains/homologies
		Microarray	Real-time PCR			1	2	3	4	5	6	7	8	
A														
1	ZK418.3	−11.4		CSN	NT				x		x		Uncharacterized	
2	F55A4.3	−7.4		CSN	DI						x		Uncharacterized	
3	K07C11.10	−6.6	−6.7	CSN				x			x		Uncharacterized	
4	C33A12.4	−6.4	−1.5	CSN							x		Putative CES-box containing	
5	C42C1.7	−5.7	−4.0	CSN, Hypodermis	DI						x	x	Acetyltransferase	
6	T26A8.2	−5.6		CSN	DI			x		x	x	x	Uncharacterized	
7	E04A4.6	−5.6	−10.0	No GFP observed		NT		x				x	Uncharacterized	
8	F10E9.1	−5.5		CSN		DD							Uncharacterized	
9	F28A12.3	−4.2	−9.2	CSN	DI						x	x	Uncharacterized	
10	F59C6.7	−4.0	−17.0	CSN		DD		x		x	x	x	IFT complex B	
11	F58E6.11	−3.1		Pharynx		NT	x						Uncharacterized	
12	C31C9.1	−3.0		CSN		NT					x	x	WD40-like beta propeller repeat	
13	F35D2.4	−2.7	−18.0	CSN		DD			x	x	x	x	Transmembrane protein 67 (Meckelin)	
14	Y53G8AM.4	−2.3		CSN		DD							E3 ubiquitin ligase	
15	M01A8.2	−2.0		Pharynx	DI			x		x			Cytoskeleton-associated protein	
16	H01G02.2	−1.8		CSN		DD			x	x	x	x	Serine/threonine kinase	
17	Y105E8A.5	−1.6	−23.0	CSN		DD		x	x	x	x	x	Bardet-Biedl syndrome protein	
18	Y39B6A.11	−1.5		CSN		DD							Protein localizing to the base of cilia	
B														
19	R102.2	−9.4		CSN		NT		x					Uncharacterized	
20	D1009.5	−7.0		CSN		DD		x		x	x	x	Dynein light chain subunit	
21	T28F3.6	−5.6		CSN		NT	x	x	x	x	x	x	RAB5-like protein	
22	K07G5.3	−4.8		CSN		NT		x		x	x	x	C2 Ca ²⁺ -binding motif-containing protein	
23	Y38F2AL.2	−4.5		CSN		DD	x	x	x		x	x	Transition zone associated protein	
24	Y41G9A.1	−3.6		CSN		DD	x	x	x	x	x	x	Murine cystic kidney disease gene Tg737 homologue	
25	M04D8.6	−3.5		CSN		DD	x		x	x			Uncharacterized	
26	C44C1.3	−3.1		CSN		NT				x			Neuronal calcium sensor protein	
27	F02D8.3	−3.0		CSN		DD		x	x	x	x	x	Dynein light intermediate chain	
28	C23H5.3	−3.0		CSN		DD				x			Uncharacterized	
29	T27B1.1	−2.9		CSN		DD		x	x	x	x	x	Intraflagellar transport 172 orthologue	
30	F20D12.3	−2.8		CSN		DD		x	x	x	x		Bardet-Biedl syndrome 2 protein	
31	T25F10.5	−2.8		CSN		DD		x	x	x	x	x	Bardet-Biedl syndrome 8 protein	
32	C27A7.4	−2.8		CSN		DD		x	x	x	x	x	Intraflagellar transport 140 homologue	
33	C18H9.8	−2.8		CSN		NT		x	x	x	x	x	Intraflagellar transport 74 homologue	
34	R01H10.6	−2.7		CSN		DD		x	x	x	x	x	Bardet-Biedl syndrome 5 protein	
35	F18C12.1	−2.6		CSN		NT		x	x	x	x	x	Dynein heavy chain (DHC) 1b isoform	
36	C54G7.4	−2.6		CSN		NT		x	x	x	x	x	WD domain containing	
37	R31.3	−2.5		CSN		DD		x	x	x	x	x	Intraflagellar transport 52 orthologue	
38	T19C4.6	−2.5		CSN		NT	x						G protein alpha subunit family of heterotrimeric GTPases	
39	C27H5.7	−2.4		CSN		DD		x	x	x	x	x	Intraflagellar transport protein	
40	F38G1.1	−2.3		CSN		DD		x	x	x	x	x	G-protein beta-like WD-40 repeats containing protein	
41	E02C12.5	−2.3		CSN		NT	x						G protein alpha subunit family of heterotrimeric GTPases	
42	F23B2.4	−2.1		CSN		DD		x	x		x	x	Intraflagellar transport 122 orthologue	
43	Y75B8A.12	−2.1		CSN		DD		x	x	x	x	x	Bardet-Biedl syndrome 7 protein	
44	F53A9.4	−2.0		CSN		NT				x			Uncharacterized	
45	K03E6.4	−2.0		CSN		DD		x		x	x	x	Transition zone associated protein	
46	R148.1	−2.0		CSN		DD		x		x	x	x	Meckel 1 (MKS-1)	
47	F19H8.3	−1.9		CSN		NT				x	x	x	ADP-ribosylation factor (ARF)-like family of protein	
48	M28.7	−1.8		CSN		NT				x	x	x	Nephrocystin-1	
49	C38D4.8	−1.6		CSN		NT					x		Human ARL6 homologue	
50	C49H3.1	−1.6		CSN		DI		x	x	x			Receptor-type guanylyl cyclase	
51	M04C9.5	−1.5		CSN		DD			x	x	x	x	MAP-kinase	

DD: DAF-19 dependence; DI: DAF-19 independence; NT: not tested.

1 - Avidor-Reiss et al., 2004.

2 - Li et al., 2004.

3 - Colosimo et al., 2004.

4 - Efimenko et al., 2005.

5 - Blacque et al., 2005.

6 - Pazour et al., 2005.

7 - Chen et al., 2006.

8 - Laurencon et al., 2007.

* Presence (X) or absence () of candidate ciliary genes in other genomic or proteomic studies.

showed a similar trend of downregulation in the *daf-19* mutant strain as displayed in the microarray experiment, although the level of downregulation for each gene varied (Table 1). Importantly, there was no change in the expression levels of any of the microarray housekeeping genes that were used as negative controls in RT-PCR experiments (*gpn-1* and *ppp-1*).

GFP expression analysis of novel candidate ciliary genes

To determine whether candidate genes identified in this study display expression patterns consistent with a role in CSNs, we conducted transcriptional reporter expression experiments. Fourteen novel candidate genes were chosen for GFP expression analyses (Table 1 and Figs. 1–3), including genes with varying degrees of signal variation in both our microarray and RT-PCR analyses, genes predicted to encode various known ciliary domains, and novel genes. Transgenic worms carrying transcriptional GFP fusion reporter constructs were generated for all genes tested and the specific temporal expression pattern for each transgenic line was determined in embryonic, larval, and adult staged worms. Eleven genes were expressed in CSNs (Figs. 1A–I; for a schematic diagram depicting CSN localization in an adult hermaphrodite worm see Fig. 1L; for *dyf-17* see Fig. 2; for *dyf-18* see Fig. 3 and Blacque et al., 2005), as expected for genes involved in cilia function. The C31C9.1 reporter construct was expressed exclusively in differentiating amphid CSNs during the 3-fold stage of embryogenesis (Fig. 1A). All other CSN-specific reporter constructs were expressed throughout all *C. elegans* developmental stages. A labial neuronal expression pattern was observed for the gene F28A12.3 (Fig. 1B). Amphid, phasmid, and labial neuronal expression patterns were observed for the genes F35D2.4, T26A8.2, ZK418.3 (Figs. 1C–E). Amphid and phasmid neuronal expression patterns were observed for the genes F55A4.3, Y53G8AM.4, and F10E9.1 (Figs. 1F–H). A more broad expression pattern in amphid neuronal and hypodermal cells was observed for the gene C42C1.7 (Fig. 1I). In contrast, only two non-CSN expression patterns were found in this candidate gene set, with both of them expressing in the pharynx (genes M01A8.2 and F58E6.11; Figs. 1J–K). Further, the reporter construct for the gene E04A4.6 showed no GFP reporter expression (data not shown). In addition, the GFP expression of a subset of the reporter genes with a CSN-specific expression pattern in a wild-type background was examined in a *daf-19* mutant background (Table 1). Taken together, our results indicate that a large subset of the genes revealed from our microarray comparisons are likely expressed and function in CSNs, similar to other ciliogenesis-specific genes.

dyf-17 encodes a novel ciliary base-associated protein that is required for ciliogenesis

Transcriptional GFP reporter constructs revealed many candidate genes with expression patterns that are consistent with the expression patterns of other experimentally verified ciliary genes. We selected two previously uncharacterized genes identified in our study to ascertain the nature of their potential ciliary functions. To provide further validation of the sensitivity of our microarray data, candidate genes that displayed only a modest level of signal downregulation in *daf-19* mutant background (DAF-19 regulation) were chosen.

We exploited the fact that ciliary gene mutations frequently result in one or more specific mutant phenotypes, including dye filling defective (Dyf), osmotic avoidance defective (Osm), and chemosensory (Che) or odorant sensation (Odr) defective phenotypes (Bargmann et al., 1993; Culotti and Russell, 1978; Starich et al., 1995). Ciliary genes that are controlled by DAF-19 are also expressed at a significantly lower level in *daf-19* mutant worms compared to wild type (Bacaj et al., 2008; Blacque et al., 2005; Chen et al., 2006; Efimenko et al., 2005; Mukhopadhyay et al., 2008; Swoboda et al., 2000; Winkelbauer et al., 2005). Thus, subjecting worms that contain mutations in any of our candidate genes

to a variety of these phenotypic or regulatory assays will likely reveal genes with cilia-specific functions.

The first gene we analyzed, Y39B6A.11, represented a strong candidate not only based on its regulation by DAF-19 (Table 1), but also because it was identified in a transposon mutagenesis screen for worms displaying an Osm phenotype (Kim Schuske, unpublished) (Bessereau et al., 2001). We subjected worms carrying the *ox175* mutant allele of the gene Y39B6A.11 to various assays indicative of cilia function and found that this mutant strain caused a modestly-penetrant dye-filling defective (Dyf) phenotype, indicative of a truncated ciliary axoneme that is not exposed to the environment (Starich et al., 1995). Similar to other ciliary genes that are regulated by DAF-19 in *C. elegans*, the promoter of Y39B6A.11 contains an X-box promoter motif (Blacque et al., 2005; Efimenko et al., 2005). Sequencing of the *ox175* mutant allele revealed that a Mos1 transposon had inserted in the third exon of this gene, likely impairing its function (YAC Y39B6A-nt 170512 / 170513; Fig. 2A). Although the *ox175* mutation maps close to the genetic position of the gene *dyf-9* on chromosome V, represented by an uncloned dye-filling defective mutant allele *n1513* (Starich et al., 1995), our complementation studies indicate that the two mutations are in separate genes (data not shown). Consequently, we assigned Y39B6A.11 the gene name *dyf-17*.

To rescue the Dyf and Osm phenotypes of *ox175* mutant animals we used a *dyf-17* genomic construct. While *ox175* mutant worms are unable to absorb the fluorescent dye Dil (Fig. 2I), *ox175* worms expressing a *dyf-17* genomic construct readily took up Dil (Fig. 2J). Similarly, the *dyf-17* (*ox175*) strain expressing this same genomic construct regained the ability to avoid high levels of osmolarity (Fig. 2K). These data unambiguously demonstrate that the Dyf and Osm phenotypes observed in *dyf-17* (*ox175*) mutants are associated with the *dyf-17* (Y39B6A.11) gene.

Transcriptional and translational *dyf-17* GFP fusion constructs were generated to determine in which CSNs the *dyf-17* gene is expressed and to reveal the subcellular localization of its gene product. Analyses of transgenic animals carrying a transcriptional GFP fusion construct demonstrated that *dyf-17* is expressed in most or all CSNs, including amphid, phasmid, and labial neurons (Fig. 2B). Expression of this same transcriptional GFP fusion construct was significantly reduced in a *daf-19* mutant background (Fig. 2E), indicating that its expression is dependent on the DAF-19 RFX transcription factor. Imaging analyses of a translational GFP fusion construct revealed that the DYF-17 protein localizes to the base of sensory cilia for both amphid (Fig. 2C) and phasmid (Fig. 2F) CSNs. We confirmed this ciliary base localization of DYF-17::GFP by comparing it, respectively, in the same transgenic animals to the ciliary base (transition zone) localization of a translational MKSR-1::tdTomato construct (Williams et al., 2011) and to the expression pattern of a transcriptional *che-13*::mCherry construct (Haycraft et al., 2003), which marks the entire CSN, including the ciliary axoneme, ciliary base, dendrite, cell body and axon (data not shown). Phenotypic analyses of transgenic worms carrying the translational GFP fusion construct in a *dyf-17* mutant background were able to rescue both the Osm (Fig. 2K) and Dyf (compare Figs. 2H, I and J) phenotypes, which confirms that the translational *dyf-17* GFP fusion construct is functional.

To determine if any obvious morphological abnormalities are present in the cilia of *dyf-17* (*ox175*) mutant worms, the overall length of cilia was assessed using soluble GFP expressed in CSNs (under the control of a *bbs-7* promoter), which marks the cell bodies, dendrites, and ciliary regions. By analyzing cilia morphologies in specific CSNs, we found that *dyf-17* (*ox175*) mutant animals contained distinctly shorter cilia than in corresponding wild-type control animals (compare Figs. 2D and G). The average length of phasmid cilia in wild-type worms is $7.11 \pm 0.18 \mu\text{m}$ ($n = 50$), whereas in *dyf-17* (*ox175*) mutants the average length is only $3.63 \pm 0.35 \mu\text{m}$ ($n = 50$) (Fig. 2L). Because the ciliary middle segment is approximately $4 \mu\text{m}$ in length, these observations suggest that *dyf-17* mutant cilia

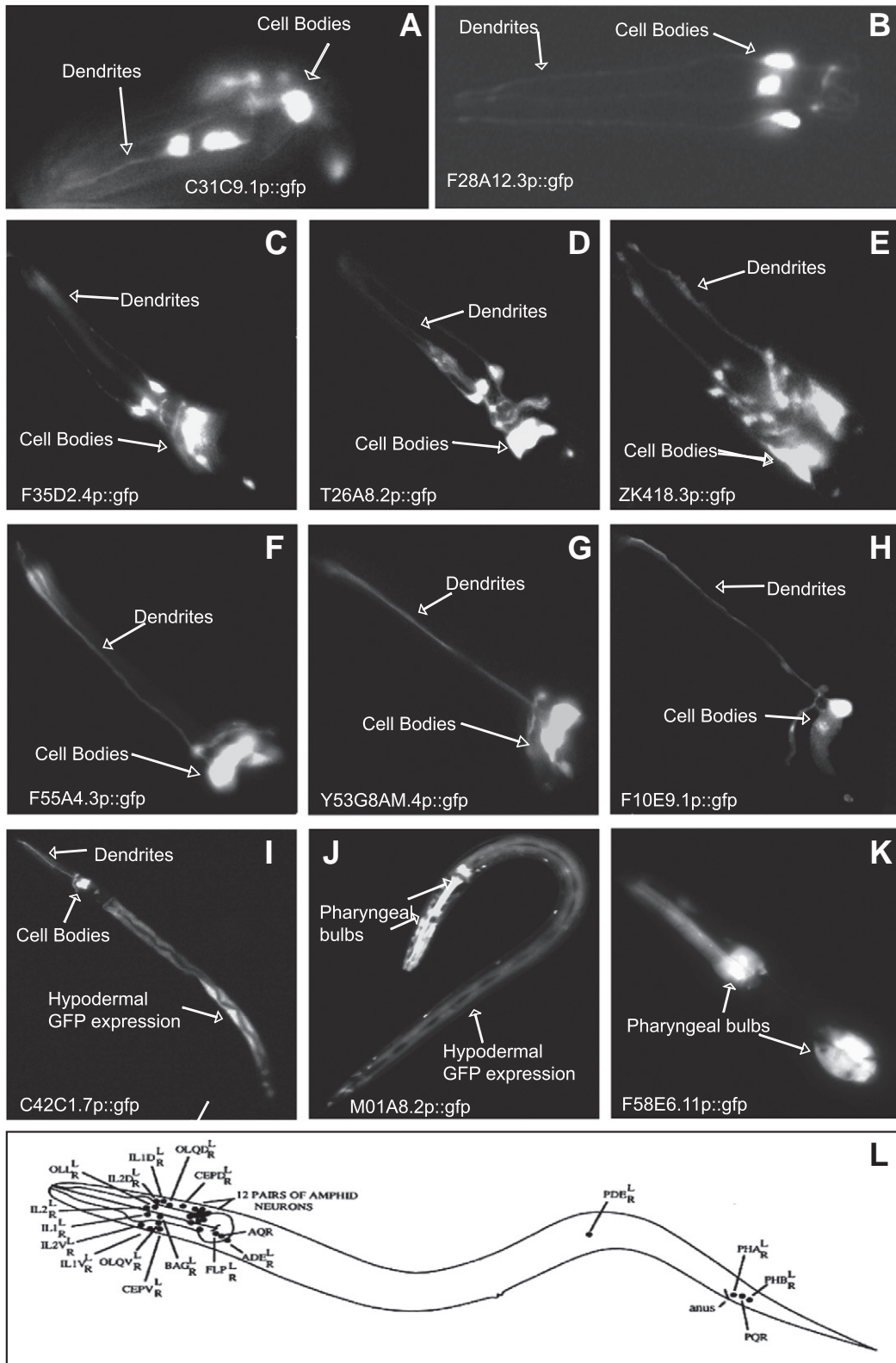


Fig. 1. Gene expression analyses using transcriptional GFP reporter fusions of select ciliary candidate genes revealed by microarrays and quantitative real-time PCR. Transgenic worms at the 3-fold embryonic stage (A) and the L1 stage (B–K) are shown: (A–H, K) head region, (I–J) whole worms. (A) C31C9.1 is expressed in amphid and labial neurons. (B) F28A12.3 is expressed exclusively in labial neurons. (C–D) F35D2.4 and T26A8.2 are expressed in amphid and labial neurons. (E) ZK418.3 is broadly expressed in head neurons, including both amphid and labial neurons. (F–H) F55A4.3, Y53G8AM.4, and F10E9.1 are expressed in amphid sensory neurons. (I) C42C1.7 has a combined amphid neuronal and hypodermal expression pattern (J–K) M01A8.2 and F58E6.11 are candidate genes lacking neuronal localization patterns. (L) A schematic diagram depicting the head (left) and tail (right) ciliated sensory neurons (CSNs).

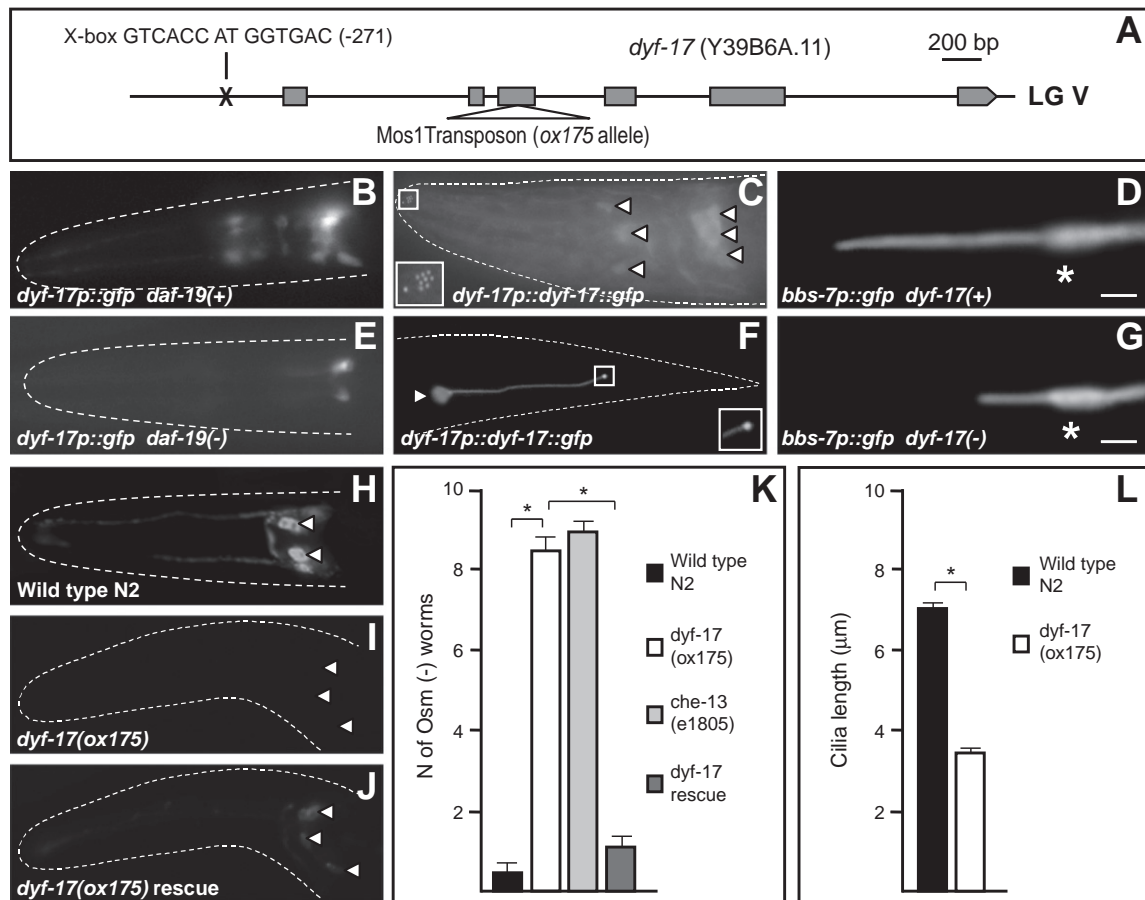


Fig. 2. Characterization of the gene *dyf-17*. (A) Schematic diagram of the *dyf-17* (Y39B6A.11) gene structure, which resides on linkage group V (LG V) in the *C. elegans* genome. Exons (boxes) and the X-box promoter motif (X) relative to the translational start site are indicated. The Mos1 transposon insertion allele *ox175* in the third exon is indicated (open arrowhead). Sequencing of the Y39B6A.11 gene in an *ox175* mutant background revealed that a Mos1 transposon had inserted in the third exon of *dyf-17* (YAC Y39B6A-nt 170512/170513). (B, E) Transcriptional reporter analyses of *dyf-17* promoter::GFP in *daf-19* (+) and *daf-19* (-) backgrounds. (C, F) Translational reporter analyses of *dyf-17* (promoter + gene) fused to GFP showing subcellular localization in amphid (C, head outlined) and phasmid (F, tail outlined) CSNs. Cutout boxes contain 2× magnified regions highlighting the ciliary base localization patterns in both amphid and phasmid neurons. (D, G) Transcriptional reporter fusion of *bbs-7*::GFP showing the length of cilia in both a wild type (full-length) and *dyf-17* (truncated) phasmid cilium. The ciliary base is demarcated (asterisk). (H–J) Dye filling assays of wild type (H), *dyf-17* mutant (*Dyf*-) animals (I) and rescued (*Dyf*+) animals (J). Worm heads are outlined (dashed lines) and amphid neuronal cell bodies are demarcated (solid arrow heads). (K) Osmotic avoidance (Osm) assay of wild type (positive control), *che-13* (negative control), *dyf-17* (mutant) and *dyf-17* rescued worms. (*) Student's t-tests: $n = 100$ for all genotypes; $p = 1.04 \times 10^{-13}$ for wild type versus *dyf-17*; $p = 3.1 \times 10^{-13}$ for *dyf-17* mutant versus *dyf-17* rescue. (L) Cilia length measurements using *bbs-7*::GFP (cf. D, G). (*) Student's t-tests: $n = 50$ for both genotypes; $p = 6.8 \times 10^{-66}$ for wild type versus *dyf-17*.

are completely missing the distal ciliary segment (Perkins et al., 1986).

To explore the possibility that the DYF-17 protein functionally interacts with other ciliary components, the localization patterns of various well-characterized ciliary proteins were determined in *dyf-17* mutant animals. Translational GFP markers selected for these analyses included IFT motor and membrane receptor proteins. The localization of the anterograde IFT motor proteins, the heterotrimeric KAP-1 subunit and homodimeric OSM-3 protein, appeared normal within the short *dyf-17* mutant cilia (Supplemental Fig. 3). Similarly, the localization patterns of several ciliary membrane proteins, including the odorant receptor ODR-10, the polycystic kidney disease-associated protein PKD-2, the G protein-coupled chemosensory receptor SRG-2, the cGMP-dependent channel TAX-2 and the TRPV channel OSM-9 appeared unaltered in the short *dyf-17* mutant cilia (Supplemental Fig. 3 and data not shown). These results do not exclude the possibility that DYF-17 may play a potentially subtle role in the ciliary processes facilitated by these genes, but raise the interesting possibility that DYF-17 has a novel ciliary function. In conclusion, we have identified a novel *C. elegans* protein that localizes at the base of cilia, where it likely functions in facilitating the formation of the ciliary distal segment.

DYF-18 is a conserved Ser/Thr kinase required for IFT and ciliogenesis

Another gene we found to be downregulated in a *daf-19* mutant background is H01G02.2 (Table 1). This gene encodes an evolutionarily conserved serine/threonine kinase of the cyclin-dependent kinase (CDK) family, with potential sequence and functional similarities to a CDK-activating kinase (CAK) whose closest human homolog is CCRK (Liu and Kipreos, 2000). A role for CCRK in ciliogenesis has been described, although the molecular mechanism by which it acts in this process remains unclear (Ko et al., 2010). Previously, we have shown that H01G02.2 contains an X-box promoter motif 159 bp upstream of the translational start site of the gene and that it is expressed exclusively in CSNs (Blacque et al., 2005; Efimenko et al., 2005). An available H01G02.2 mutant allele, *ok200*, represents a 1.25 kb deletion which removes the promoter region containing the X-box, the first exon and part of the second exon.

We subjected the *ok200* mutant strain to cilia-related phenotypic analyses. To identify possible structural abnormalities of cilia, we tested the ability of the strain to take up the fluorescent dye Dil. Compared to wild-type animals, *ok200* mutant animals display only a weak ability to uptake the dye in amphid (head) and phasmid (tail) neurons (Figs. 3A, B). The *Dyf* phenotype was quantified and found to

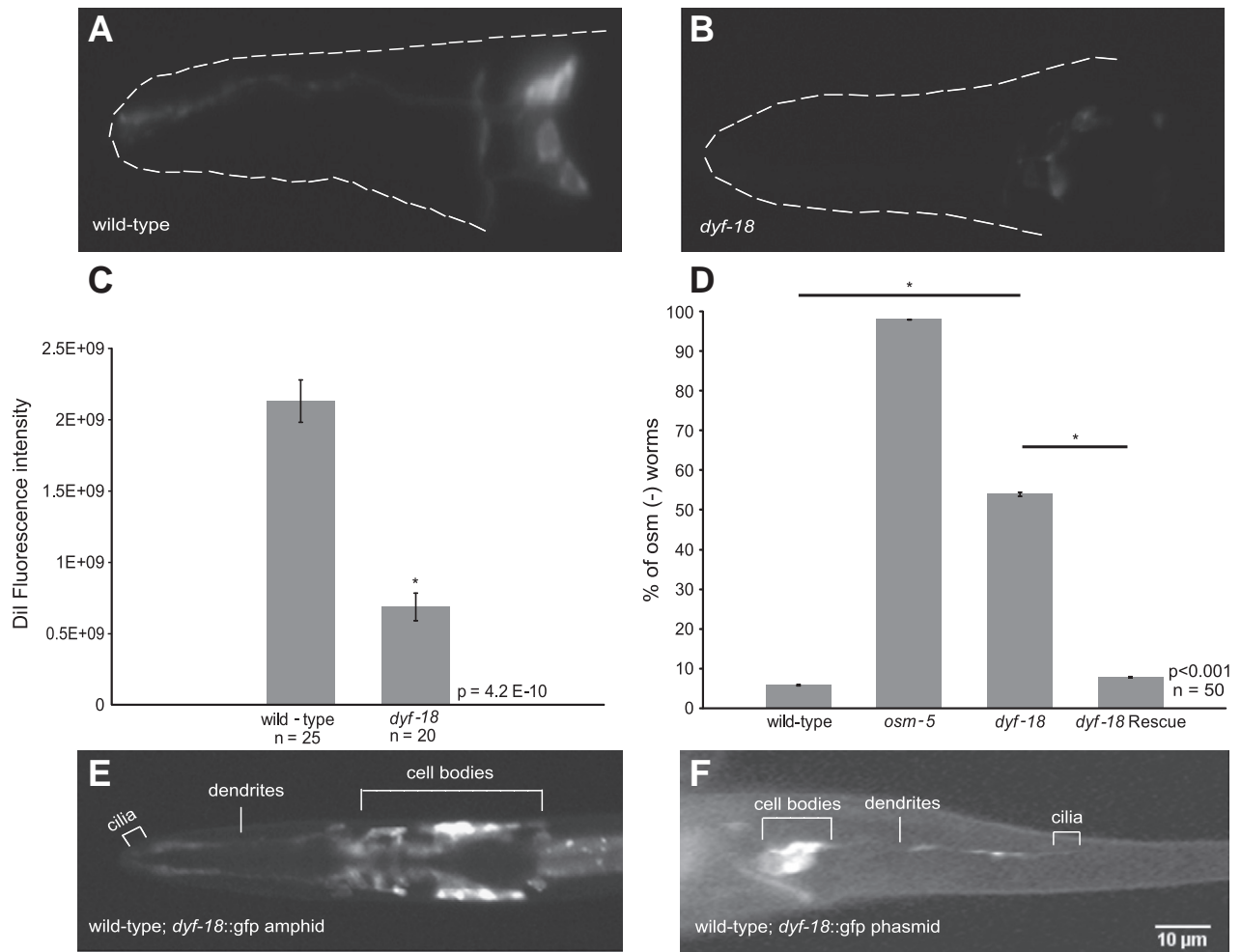


Fig. 3. DYF-18 is an evolutionarily conserved CDK/CCRK/LF2p-related Ser/Thr kinase required for proper cilium-dependent fluorescent dye filling and chemosensation. (A, B) Fluorescence images of the head region of wild type and *dyf-18* (*ok200*) mutant worms, respectively, taken at the same exposure time after a dye filling assay. *dyf-18* mutant animals show weak dye-filling defects in amphid neurons (not shown for phasmid neurons). (C) Quantification of the fluorescent dye filling defects, showing a statistically significant decrease in the dye uptake in a *dyf-18* mutant strain as compared to wild type. (D) *dyf-18* mutants display an osmotic avoidance defective (Osm) phenotype that is rescued by introduction of a DYF-18::GFP translational fusion construct. Wild type serves as a positive control, *osm-5* mutants serve as a negative control. (C, D) n denotes the number of animals tested. (*) Student's t-tests were performed for statistical significance (p values are shown). (E, F) Expression pattern and localization of the DYF-18 protein in head and tail neurons, respectively. A DYF-18::GFP translational fusion construct is expressed in amphid, phasmid and labial neurons in wild-type animals. The encoded protein localizes diffusely within the cell bodies, dendrites, and ciliary compartments. Cell bodies, dendrites and ciliary regions are indicated.

be statistically significant (Fig. 3C). Next, we determined that the *ok200* mutant strain displays a chemosensory defect. Specifically, the strain was impaired in its ability to avoid substances of high osmolarity (Osm phenotype), similar both to *dyf-17* mutants and a control (*osm-5*) mutant strain (Fig. 3D). Importantly, the Osm phenotype displayed by *ok200* mutants could be fully rescued by expression of a wild-type copy of the gene fused to GFP (Fig. 3D), demonstrating that the translational GFP fusion protein is functional. Based on these data, we assigned the name *dyf-18* to the H01G02.2 gene.

To determine the subcellular localization of the DYF-18 protein, we expressed a DYF-18::GFP translational fusion. The construct was expressed exclusively in most CSNs (including amphid, phasmid and labial neurons), as expected from its regulation by DAF-19 (Table 1). The encoded fusion protein was largely cytoplasmic, with diffuse fluorescence in the cell bodies, dendrites, and within ciliary compartments (Figs. 3E, F). No specific enrichment of the protein within cilia was observed, similar to that reported for DYF-5, a *C. elegans* MAP kinase known to affect cilia function (Burghoorn et al., 2007).

To visualize potential abnormalities in cilia and the localization of IFT proteins, we generated several transgenic strains that express in a *dyf-18* (*ok200*) mutant background various GFP-tagged IFT protein

markers, namely the anterograde IFT motor components KAP-1 and OSM-3, the IFT subcomplex A protein CHE-11, and the IFT subcomplex B proteins CHE-2 and OSM-5. Although we found that the structure of most cilia appeared superficially similar to wild type, with occasionally long curved cilia, we noted abnormalities in the distribution of some IFT proteins. Specifically, the *dyf-18* (*ok200*) mutant showed prominent accumulations of the homodimeric kinesin-II motor, OSM-3, between the middle and the distal segment both in the amphid and phasmid neuron cilia in 100% of the mutant worms (Fig. 4). The IFT protein OSM-5, on the other hand, was frequently observed to accumulate at the base of cilia in amphid and phasmid neurons, with much reduced localization along the ciliary axoneme (Fig. 4). Interestingly, not all IFT proteins tested were significantly affected. Both CHE-11 and CHE-2 displayed essentially wild-type localization to both the middle and distal segments, and could be observed to undergo seemingly normal IFT.

Together, our data suggest that DYF-18, a CDK7/CCRK/LF2p-related serine/threonine kinase found exclusively in CSNs, modulates the behavior and function of at least some IFT proteins, explaining its importance in the formation and function of cilia. Additional studies will be required to understand the precise role of DYF-18 in IFT,

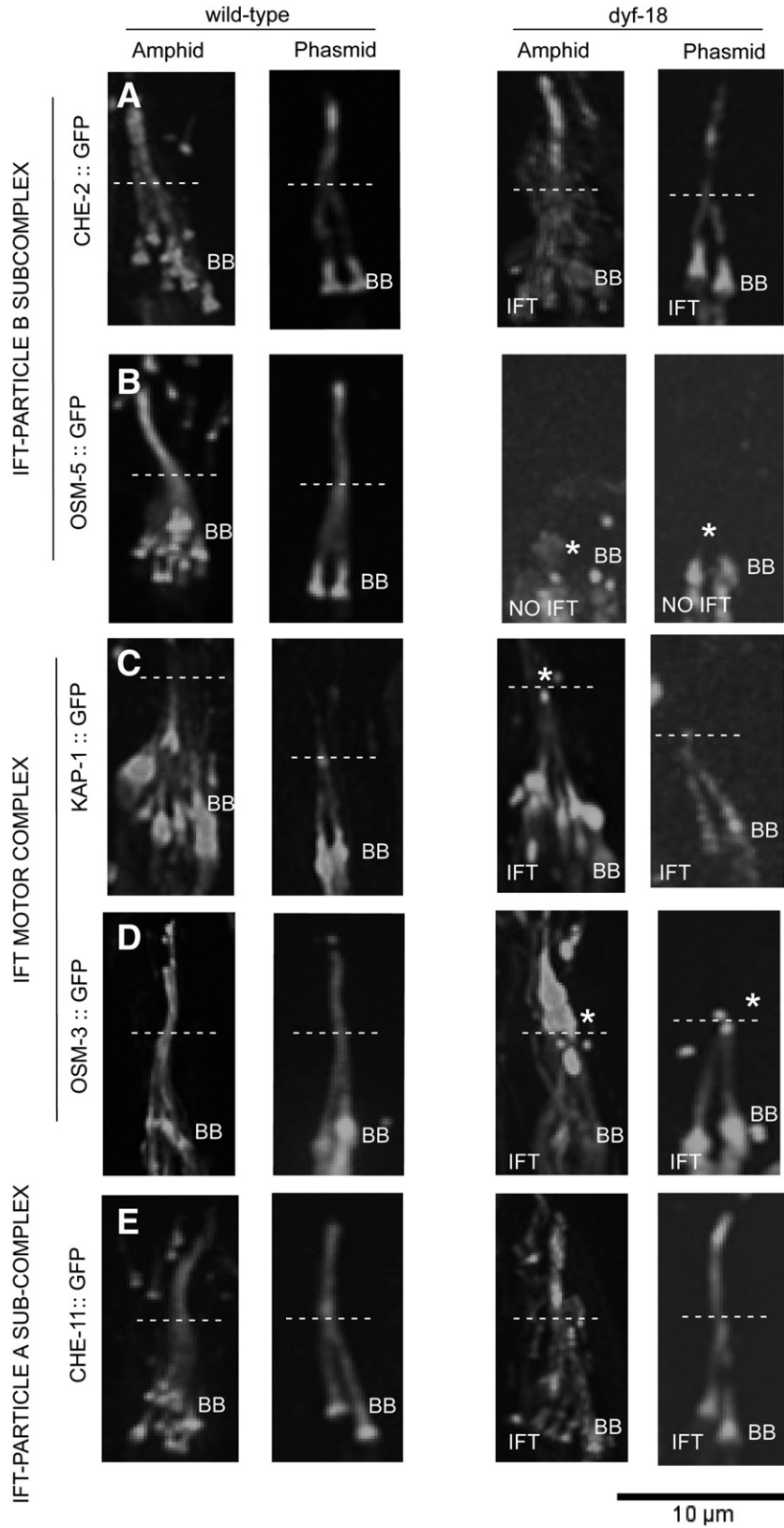


Fig. 4. DYF-18 regulates the localization of intraflagellar transport (IFT) machinery components. Both amphid and phasmid cilia are shown. (A, B) Localization of IFT subcomplex B proteins. CHE-2 shows wild-type localization whereas OSM-5 is largely excluded from cilia and accumulates at the base of cilia. (C, D) Localization of IFT motors. KAP-1 shows essentially wild-type localization with occasional accumulations at the tip of the middle segment (marked by *) whereas the OSM-3 motor is largely unable to enter the distal segment and shows large accumulations (marked by *) between the middle and the distal segment. (E) Shows the essentially normal localization of the IFT subcomplex A protein CHE-11 to the middle and distal ciliary segments. In all panels the dotted line divides the middle and the distal segments. BB, degenerate basal bodies; *, marks protein accumulation. Presence or absence of IFT in the mutant has been denoted.

including a possible functional redundancy with the DYF-5 kinase that is known to regulate IFT activity (Burghoorn et al., 2007).

Discussion

To identify novel genes involved in cilia-related functions, microarray expression profiles of *daf-19* (+) and *daf-19* (–) worms were compared using RNA extracted from embryos at a developmental stage when ciliogenesis and cilia assembly are still ongoing in most CSNs. Validation for this approach was in part provided through the identification of numerous internal positive controls, which included genes that have been previously implicated in a variety of cilia-related processes. Importantly however, several novel ciliary gene candidates were additionally revealed in this analysis, a subset of which were subsequently shown to have cilia-specific expression patterns and functions. In particular, we identify two novel ciliogenic proteins, DYF-17 and DYF-18. The *dyf-17* gene, which is required for proper ciliary assembly, is expressed exclusively in CSNs and encodes a protein that localizes to the base (transition zone) of cilia. The *dyf-18* gene encodes a Ser/Thr kinase and is important for the fidelity of intraflagellar transport (IFT), and thus, cilium formation and function. The DYF-18 protein localizes to the cell body, dendrite, and cilia of most CSNs. Hence, data revealed in these developmental-specific microarray analyses will be useful for the further identification of evolutionarily conserved genes required for the assembly, regulation, and function of cilia.

Temporal-specific expression of many genes occurs during the development of the *C. elegans* embryo. Specifically, ciliogenesis is largely initiated before the end of the 2-fold stage of embryogenesis (Heiman and Shaham, 2009; Senti and Swoboda, 2008; Sulston et al., 1983), which prompted us to use RNA isolated from worms at the early 3-fold stage of embryogenesis for microarray and subsequent RT-PCR analyses. The *C. elegans* embryo at the 3-fold stage contains fewer than 600 cells, including about 50 CSNs (Sulston et al., 1983). Thus, while cilia-specific transcripts may be expressed in less than 10% of the total number of cells, comparisons of embryos from two distinct genetic backgrounds, *daf-19* (+) and (–), successfully revealed genes enriched in cilia functions. A subset of the novel genes identified in these microarray analyses were further shown to contain cilia-specific expression patterns and functions using a combination of RT-PCR comparisons, transcriptional GFP fusion expression studies, and the characterization of candidate genes. It should be noted that the data presented here, which utilized a highly synchronized 3-fold stage embryonic population, are complementary to a similar study that utilized a mixed stage population comparing RNA extracted from the same strains (Chen et al., 2006). As expected, many genes were identified in both analyses, including 23 of the 32 characterized IFT genes present in the *C. elegans* genome. However, several candidate genes were more highly enriched in the present analyses, which likely reflect the enhanced expression of certain ciliary genes during embryonic development. For example, a transcriptional GFP fusion of the C31C9.1 gene, revealed an embryonic-specific expression pattern in CSNs during the 3-fold stage of embryogenesis. This result strongly supports the notion of temporal-specific variation in the expression level of certain cilia-specific genes at the time of ciliogenesis. Overall, our transcriptional profiling of tightly staged embryos allowed for the discovery of a large number of potentially new cilia-specific genes. Using a cutoff of at least 1.5-fold signal variation, the overlap between the previous (Chen et al., 2006) and our present study is only 179/881 candidate genes (Supplemental Table 2). Added sensitivity is exemplified by the fact that of the candidate genes with known expression patterns (www.wormbase.org), 3.6% (found by Chen et al., 2006) as opposed to 8.0% (found in our present study) were expressed exclusively in CSNs. Key numbers like these indicate that our present study will be a rich resource for the discovery of new cilia-specific genes.

The genes identified in our present analyses were compared to lists of genes that previously and successfully have been used to reveal genes

involved in cilia-related functions. Data from these previous studies, which have utilized a combination of bioinformatic, proteomic, and comparative genomics-based approaches, have been compiled into ciliary gene databases (Arnaiz et al., 2009; Gherman et al., 2006; Inglis et al., 2006). Comparisons of the results from our study with the genes present in these ciliary gene databases revealed that many of the genes identified here have been additionally described in other previous studies. For example, 33 of the genes that were shown to contain a statistically significant variation in expression in our analyses were additionally found in at least three independent candidate ciliary gene lists (Table 1, Supplemental Table 2). This further confirms that the microarray analysis presented in our study is enriched with genes involved in cilia and cilia-related functions.

Several genes with homologs that have been previously implicated in the pathology of numerous cilia-related human genetic disorders, called ciliopathies, were found to contain a statistically significant difference in the level of expression in our study. This includes five genes that have been implicated in the pleiotropic human genetic disorder Bardet–Biedl syndrome, including *bbs-1*, *-2*, *-5*, *-8*, and *-9* (Zaghoul and Katsanis, 2009). Four genes were identified that when defective are responsible for causing Meckel–Gruber syndrome, namely *mks-1* and *mks-3*, and potentially also *mksr-1* and *mksr-2*. Furthermore, the gene *nph-1*, which when defective causes Nephrophthisis (Winkelbauer et al., 2005), was also identified. Thus, further analysis of novel genes identified in our study is likely to reveal additional uncharacterized genes implicated in potentially new ciliopathies.

Molecular and phenotypic characterizations of the Y39B6A.11 and H01G02.2 loci in *C. elegans* uncovered two ciliogenic genes, *dyf-17* and *dyf-18*, respectively. Mutations in either of these genes resulted in both dye-filling (Dyf) and osmotic avoidance (Osm) defects. *dyf-17* and *dyf-18* each have an X-box promoter motif 271 bp and 159 bp upstream of the start codon, respectively, similar to other ciliary genes that are under the direct transcriptional control by the DAF-19 RFX transcription factor. Consistent with the presence of X-boxes, the expression of the *dyf-17* and *dyf-18* genes is significantly reduced in a *daf-19* mutant background.

While the DYF-17 protein is highly conserved within *Caenorhabditis* species, it does not appear to be present outside of nematodes and as of yet, does not contain any domains of known function (data not shown). DYF-17 localizes to the ciliary base (transition zone) and – based on the mutant phenotypes of the *dyf-17* gene – is required for forming or maintaining full-length cilia. This unique combination of protein localization and mutant phenotype further underscores the importance of the ciliary base for formation and development of the cilium. The ciliary base serves as a selective protein-sorting hub for proteins slated to enter the cilium proper (Craigie et al., 2010; Rosenbaum and Witman, 2002). We speculate that DYF-17 may be involved in mechanisms that permit ciliary protein entry into the cilium. Upon *dyf-17* mutation this process is curtailed and subsequently leads to shortened cilia. Our results collectively indicate that DYF-17 may play a unique role at the base of *C. elegans* cilia.

DYF-18 is an evolutionarily well-conserved serine/threonine protein kinase expressed in CSNs, which is required for ciliogenesis, likely because it modulates the IFT process. Specifically, abrogating DYF-18 appears to selectively affect the function of some (but not all) IFT components, including the anterograde kinesin motor OSM-3. Similar to DYF-5, another known *C. elegans* kinase that affects IFT (Burghoorn et al., 2007), DYF-18 appears largely cytosolic, with no specific enrichment in cilia. DYF-18 is related to the human cell cycle related kinase (CCRK), a likely homolog of LF2p (flagella length mutant) in *Chlamydomonas* (Ko et al., 2010; Liu and Kipreos, 2000). CCRK has been shown to physically interact with Broad-minded or Bromi (a TBC-domain containing protein), and is required for proper cilia assembly and ciliary length in vertebrates (Ko et al., 2010). Although LF2p and CCRK have to date not been directly associated with IFT, our results suggest that this class of kinases may be generally

involved in controlling ciliogenesis/cilium length in a manner dependent on IFT, which is required for building and maintaining cilia (Silverman and Leroux, 2009). Intriguingly, disruption of DYF-18 causes the anterograde IFT motor OSM-3 to accumulate between the middle and distal segments, a phenotype also observed in the *dyf-5* kinase mutant (Burghoorn et al., 2007). *dyf-5* encodes a homologue of LF4p, which like LF2p, is required for cilium length control (Asleson and Lefebvre, 1998; Berman et al., 2003; Burghoorn et al., 2007). Whether DYF-18, similar to DYF-5, is involved in modulating the correct association between different IFT components and the motors, and the proper behavior of the motors themselves, will require further investigation.

In conclusion, our transcriptional profiling of the DAF-19 RFX transcription factor at the time when ciliogenic processes are most prevalent has uncovered numerous known and new candidate ciliary genes. In addition to helping uncover a complete molecular parts list required for cilium structure and function, our findings also reveal a novel ciliary base protein important for cilium formation and that an evolutionarily conserved kinase of the CDK/CCRK/LF2p family regulates cilium formation by modulating the function of the IFT machinery.

Supplementary materials related to this article can be found online at doi:10.1016/j.ydbio.2011.06.028.

Acknowledgments

We thank Thomas Bürglin, Patrick Dessi, Krishanu Mukherjee, Limin Hao and Gabriele Senti for technical help and helpful discussions. Anthony Wright assisted in quantitative real-time PCR. Elizabeth De Stasio provided valuable comments on experiments and the manuscript. We thank the *Caenorhabditis* Genetics Center, which is funded by the National Institutes of Health, for providing some of the worm strains used in this study. M.R.L. is a Michael Smith Foundation for Health Research (MSFHR) senior scholar. M.R.L. acknowledges financial support from the Canadian Institutes of Health Research (CIHR grant MOP-82870) and the March of Dimes. J.B. was supported by a fellowship from the Carl Trygger Foundation. B.P.P. was supported by a Fulbright Fellowship and by a Stiftelse Lars Hiertas Minne grant. Work in the laboratory of P.S., a member of the NordForsk Nordic *C. elegans* and cilia networks, was supported by grants from the Swedish Research Council and from the Swedish Foundation for Strategic Research.

References

Adams, N.A., Awadein, A., Toma, H.S., 2007. The retinal ciliopathies. *Ophthalmic Genet.* 28, 113–125.

Arnaiz, O., Malinowska, A., Klotz, C., Sperling, L., Dadlez, M., Koll, F., Cohen, J., 2009. Cildb: a Knowledgebase for Centrosomes and Cilia. Database, Oxford. bap022.

Asleson, C.M., Lefebvre, P.A., 1998. Genetic analysis of flagellar length control in *Chlamydomonas reinhardtii*: a new long-flagella locus and extragenic suppressor mutations. *Genetics* 148, 693–702.

Avidor-Reiss, T., Maer, A.M., Koundakjian, E., Polyanovsky, A., Keil, T., Subramaniam, S., Zuker, C.S., 2004. Decoding cilia function: defining specialized genes required for compartmentalized cilia biogenesis. *Cell* 117, 527–539.

Baas, D., Meiniel, A., Benadiba, C., Bonnafé, E., Meiniel, O., Reith, W., Durand, B., 2006. A deficiency in RFX3 causes hydrocephalus associated with abnormal differentiation of ependymal cells. *Eur. J. Neurosci.* 24, 1020–1030.

Bacaj, T., Lu, Y., Shaham, S., 2008. The conserved proteins CHE-12 and DYF-11 are required for sensory cilium function in *Caenorhabditis elegans*. *Genetics* 178, 989–1002.

Bargmann, C.I., Hartwig, E., Horvitz, H.R., 1993. Odorant-selective genes and neurons mediate olfaction in *C. elegans*. *Cell* 74, 515–527.

Barrett, T., Edgar, R., 2006. Mining microarray data at NCBI's Gene Expression Omnibus (GEO)*. *Methods Mol. Biol.* 338, 175–190.

Berman, S.A., Wilson, N.F., Haas, N.A., Lefebvre, P.A., 2003. A novel MAP kinase regulates flagellar length in *Chlamydomonas*. *Curr. Biol.* 13, 1145–1149.

Bessereau, J.L., Wright, A., Williams, D.C., Schuske, K., Davis, M.W., Jorgensen, E.M., 2001. Mobilization of a *Drosophila* transposon in the *Caenorhabditis elegans* germ line. *Nature* 413, 70–74.

Bialas, N.J., Inglis, P.N., Li, C., Robinson, J.F., Parker, J.D., Healey, M.P., Davis, E.E., Inglis, C.D., Toivonen, T., Cottell, D.C., Blacque, O.E., Quarmby, L.M., Katsanis, N., Leroux, M.R., 2009. Functional interactions between the ciliopathy-associated Meckel syndrome 1

(MKS1) protein and two novel MKS1-related (MKSR) proteins. *J. Cell Sci.* 122, 611–624.

Blacque, O.E., Cevik, S., Kaplan, O.I., 2008. Intraflagellar transport: from molecular characterisation to mechanism. *Front. Biosci.* 13, 2633–2652.

Blacque, O.E., Perens, E.A., Borojevich, K.A., Inglis, P.N., Li, C., Warner, A., Khattra, J., Holt, R.A., Ou, G., Mah, A.K., McKay, S.J., Huang, P., Swoboda, P., Jones, S.J., Marra, M.A., Baillie, D.L., Moerman, D.G., Shaham, S., Leroux, M.R., 2005. Functional genomics of the cilium, a sensory organelle. *Curr. Biol.* 15, 935–941.

Blacque, O.E., Reardon, M.J., Li, C., McCarthy, J., Mahjoub, M.R., Ansley, S.J., Badano, J.L., Mah, A.K., Beales, P.L., Davidson, W.S., Johnsen, R.C., Audeh, M., Plasterk, R.H., Baillie, D.L., Katsanis, N., Quarmby, L.M., Wicks, S.R., Leroux, M.R., 2004. Loss of *C. elegans* BBS-7 and BBS-8 protein function results in cilia defects and compromised intraflagellar transport. *Genes Dev.* 18, 1630–1642.

Brenner, S., 1974. The genetics of *Caenorhabditis elegans*. *Genetics* 77, 71–94.

Burghoorn, J., Dekkers, M.P., Rademakers, S., de Jong, T., Willemsen, R., Jansen, G., 2007. Mutation of the MAP kinase DYF-5 affects docking and undocking of kinesin-2 motors and reduces their speed in the cilia of *Caenorhabditis elegans*. *Proc. Natl. Acad. Sci. U.S.A.* 104, 7157–7162.

Cevik, S., Hori, Y., Kaplan, O.I., Kida, K., Toivonen, T., Foley-Fisher, C., Cottell, D., Katada, T., Kontani, K., Blacque, O.E., 2010. Joubert syndrome Arl13b functions at ciliary membranes and stabilizes protein transport in *Caenorhabditis elegans*. *J. Cell Biol.* 188, 953–969.

Chen, N., Mah, A., Blacque, O.E., Chu, J., Phgora, K., Bakhoun, M.W., Newbury, C.R., Khattra, J., Chan, S., Go, A., Efimenko, E., Johnsen, R., Phirke, P., Swoboda, P., Marra, M., Moerman, D.G., Leroux, M.R., Baillie, D.L., Stein, L.D., 2006. Identification of ciliary and ciliopathy genes in *Caenorhabditis elegans* through comparative genomics. *Genome Biol.* 7, R126.

Christensen, S.T., Pedersen, S.F., Satir, P., Veland, I.R., Schneider, L., 2008. The primary cilium coordinates signaling pathways in cell cycle control and migration during development and tissue repair. *Curr. Top. Dev. Biol.* 85, 261–301.

Chu, J.S., Baillie, D.L., Chen, N., 2010. Convergent evolution of RFX transcription factors and ciliary genes predated the origin of metazoans. *BMC Evol. Biol.* 10, 130.

Colosimo, M.E., Brown, A., Mukhopadhyay, S., Gabel, C., Lanjuin, A.E., Samuel, A.D., Sengupta, P., 2004. Identification of thermosensory and olfactory neuron-specific genes via expression profiling of single neuron types. *Curr. Biol.* 14, 2245–2251.

Cortellino, S., Wang, C., Wang, B., Bassi, M.R., Caretti, E., Champeval, D., Calmont, A., Jarnik, M., Burch, J., Zaret, K.S., Larue, L., Bellacosa, A., 2009. Defective ciliogenesis, embryonic lethality and severe impairment of the Sonic Hedgehog pathway caused by inactivation of the mouse complex A intraflagellar transport gene *Ift122/Wdr10*, partially overlapping with the DNA repair gene *Med1/Mbd4*. *Dev. Biol.* 325, 225–237.

Craigie, B., Tsao, C.C., Diener, D.R., Hou, Y., Lechtreck, K.F., Rosenbaum, J.L., Witman, G.B., 2010. CEP290 tethers flagellar transition zone microtubules to the membrane and regulates flagellar protein content. *J. Cell Biol.* 190, 927–940.

Culotti, J.G., Russell, R.L., 1978. Osmotic avoidance defective mutants of the nematode *Caenorhabditis elegans*. *Genetics* 90, 243–256.

Davis, E.E., Brueckner, M., Katsanis, N., 2006. The emerging complexity of the vertebrate cilium: new functional roles for an ancient organelle. *Dev. Cell* 11, 9–19.

Dennis Jr., G., Sherman, B.T., Hosack, D.A., Yang, J., Gao, W., Lane, H.C., Lempicki, R.A., 2003. DAVID: database for annotation, visualization, and integrated discovery. *Genome Biol.* 4, P3.

Efimenko, E., Bubbs, K., Mak, H.Y., Holzman, T., Leroux, M.R., Ruvkun, G., Thomas, J.H., Swoboda, P., 2005. Analysis of *xbx* genes in *C. elegans*. *Development* 132, 1923–1934.

El Zein, L., Ait-Lounis, A., Morle, L., Thomas, J., Chhin, B., Spassky, N., Reith, W., Durand, B., 2009. RFX3 governs growth and beating efficiency of motile cilia in mouse and controls the expression of genes involved in human ciliopathies. *J. Cell Sci.* 122, 3180–3189.

Gherman, A., Davis, E.E., Katsanis, N., 2006. The ciliary proteome database: an integrated community resource for the genetic and functional dissection of cilia. *Nat. Genet.* 38, 961–962.

Haycraft, C.J., Schafer, J.C., Zhang, Q., Taulman, P.D., Yoder, B.K., 2003. Identification of CHE-13, a novel intraflagellar transport protein required for cilia formation. *Exp. Cell Res.* 284, 251–263.

Haycraft, C.J., Swoboda, P., Taulman, P.D., Thomas, J.H., Yoder, B.K., 2001. The *C. elegans* homolog of the murine cystic kidney disease gene *Tg737* functions in a ciliogenic pathway and is disrupted in *osm-5* mutant worms. *Development* 128, 1493–1505.

Heiman, M.G., Shaham, S., 2009. DEX-1 and DYF-7 establish sensory dendrite length by anchoring dendritic tips during cell migration. *Cell* 137, 344–355.

Hobert, O., 2002. PCR fusion-based approach to create reporter gene constructs for expression analysis in transgenic *C. elegans*. *Biotechniques* 32, 728–730.

Howard, P.W., Howard, T.L., Maurer, R.A., 2010. Generation of mice with a conditional allele for *Ift172*. *Transgenic Res.* 19, 121–126.

Inglis, P.N., Borojevich, K.A., Leroux, M.R., 2006. Piecing together a ciliome. *Trends Genet.* 22, 491–500.

Jauregui, A.R., Nguyen, K.C., Hall, D.H., Barr, M.M., 2008. The *Caenorhabditis elegans* nephrocystins act as global modifiers of cilium structure. *J. Cell Biol.* 180, 973–988.

Johnson, J.L., Leroux, M.R., 2010. cAMP and cGMP signaling: sensory systems with prokaryotic roots adopted by eukaryotic cilia. *Trends Cell Biol.* 20, 435–444.

Ko, H.W., Norman, R.X., Tran, J., Fuller, K.P., Fukuda, M., Eggenschwiler, J.T., 2010. Broad-minded links cell cycle-related kinase to cilia assembly and hedgehog signal transduction. *Dev. Cell* 18, 237–247.

Kunitomo, H., Uesugi, H., Kohara, Y., Iino, Y., 2005. Identification of ciliated sensory neuron-expressed genes in *Caenorhabditis elegans* using targeted pull-down of poly (A) tails. *Genome Biol.* 6, R17.

Lancaster, M.A., Louie, C.M., Silhavy, J.L., Sintasath, L., Decambre, M., Nigam, S.K., Willert, K., Gleeson, J.G., 2009. Impaired Wnt-beta-catenin signaling disrupts adult renal homeostasis and leads to cystic kidney ciliopathy. *Nat. Med.* 15, 1046–1054.

- Laurencon, A., Dubruille, R., Efimenko, E., Grenier, G., Bissett, R., Cortier, E., Rolland, V., Swoboda, P., Durand, B., 2007. Identification of novel regulatory factor X (RFX) target genes by comparative genomics in *Drosophila* species. *Genome Biol.* 8, R195.
- Li, J.B., Gerdes, J.M., Haycraft, C.J., Fan, Y., Teslovich, T.M., May-Simera, H., Li, H., Blacque, O. E., Li, L., Leitch, C.C., Lewis, R.A., Green, J.S., Parfrey, P.S., Leroux, M.R., Davidson, W.S., Beales, P.L., Guay-Woodford, L.M., Yoder, B.K., Stormo, G.D., Katsanis, N., Dutcher, S.K., 2004. Comparative genomics identifies a flagellar and basal body proteome that includes the BBS5 human disease gene. *Cell* 117, 541–552.
- Li, Y., Wei, Q., Zhang, Y., Ling, K., Hu, J., 2010. The small GTPases ARL-13 and ARL-3 coordinate intraflagellar transport and ciliogenesis. *J. Cell Biol.* 189, 1039–1051.
- Liu, J., Kipreos, E.T., 2000. Evolution of cyclin-dependent kinases (CDKs) and CDK-activating kinases (CAKs): differential conservation of CAKs in yeast and metazoa. *Mol. Biol. Evol.* 17, 1061–1074.
- Marshall, W.F., Nonaka, S., 2006. Cilia: tuning in to the cell's antenna. *Curr. Biol.* 16, R604–R614.
- McKay, S.J., Johnsen, R., Khattra, J., Asano, J., Baillie, D.L., Chan, S., Dube, N., Fang, L., Goszczynski, B., Ha, E., Halfnight, E., Hollebakk, R., Huang, P., Hung, K., Jensen, V., Jones, S.J., Kai, H., Li, D., Mah, A., Marra, M., McGhee, J., Newbury, R., Pouzyrev, A., Riddle, D.L., Sonhammer, E., Tian, H., Tu, D., Tyson, J.R., Vatcher, G., Warner, A., Wong, K., Zhao, Z., Moerman, D.G., 2003. Gene expression profiling of cells, tissues, and developmental stages of the nematode *C. elegans*. *Cold Spring Harb. Symp. Quant. Biol.* 68, 159–169.
- Mello, C.C., Kramer, J.M., Stinchcomb, D., Ambros, V., 1991. Efficient gene transfer in *C. elegans*: extrachromosomal maintenance and integration of transforming sequences. *EMBO J.* 10, 3959–3970.
- Moussaif, M., Sze, J.Y., 2009. Intraflagellar transport/Hedgehog-related signaling components couple sensory cilium morphology and serotonin biosynthesis in *Caenorhabditis elegans*. *J. Neurosci.* 29, 4065–4075.
- Mukhopadhyay, S., Lu, Y., Shaham, S., Sengupta, P., 2008. Sensory signaling-dependent remodeling of olfactory cilia architecture in *C. elegans*. *Dev. Cell* 14, 762–774.
- Pazour, G.J., Agrin, N., Leszyk, J., Witman, G.B., 2005. Proteomic analysis of a eukaryotic cilium. *J. Cell Biol.* 170, 103–113.
- Pedersen, L.B., Rosenbaum, J.L., 2008. Intraflagellar transport (IFT) role in ciliary assembly, resorption and signalling. *Curr. Top. Dev. Biol.* 85, 23–61.
- Perkins, L.A., Hedgecock, E.M., Thomson, J.N., Culotti, J.G., 1986. Mutant sensory cilia in the nematode *Caenorhabditis elegans*. *Dev. Biol.* 117, 456–487.
- Piasecki, B.P., Burghoorn, J., Swoboda, P., 2010. Regulatory Factor X (RFX)-mediated transcriptional rewiring of ciliary genes in animals. *Proc. Natl. Acad. Sci. U.S.A.* 107, 12969–12974.
- Qin, H., Burnette, D.T., Bae, Y.K., Forscher, P., Barr, M.M., Rosenbaum, J.L., 2005. Intraflagellar transport is required for the vectorial movement of TRPV channels in the ciliary membrane. *Curr. Biol.* 15, 1695–1699.
- Ramakers, C., Ruijter, J.M., Deprez, R.H., Moorman, A.F., 2003. Assumption-free analysis of quantitative real-time polymerase chain reaction (PCR) data. *Neurosci. Lett.* 339, 62–66.
- Rashid, S., Grzmil, P., Drenckhahn, J.D., Meinhardt, A., Adham, I., Engel, W., Neesen, J., 2010. Disruption of the murine dynein light chain gene *Tcte3-3* results in asthenozoospermia. *Reproduction* 139, 99–111.
- Rosenbaum, J.L., Witman, G.B., 2002. Intraflagellar transport. *Nat. Rev. Mol. Cell Biol.* 3, 813–825.
- Scholey, J.M., 2008. Intraflagellar transport motors in cilia: moving along the cell's antenna. *J. Cell Biol.* 180, 23–29.
- Senti, G., Ezcurra, M., Lobner, J., Schafer, W.R., Swoboda, P., 2009. Worms with a single functional sensory cilium generate proper neuron-specific behavioral output. *Genetics* 183, 595–605.
- Senti, G., Swoboda, P., 2008. Distinct isoforms of the RFX transcription factor DAF-19 regulate ciliogenesis and maintenance of synaptic activity. *Mol. Biol. Cell* 19, 5517–5528.
- Shah, A.S., Ben-Shahar, Y., Moninger, T.O., Kline, J.N., Welsh, M.J., 2009. Motile cilia of human airway epithelia are chemosensory. *Science* 325, 1131–1134.
- Shulzhenko, N., Yambartsev, A., Goncalves-Primo, A., Gerbase-DeLima, M., Morgun, A., 2005. Selection of control genes for quantitative RT-PCR based on microarray data. *Biochem. Biophys. Res. Commun.* 337, 306–312.
- Silverman, M.A., Leroux, M.R., 2009. Intraflagellar transport and the generation of dynamic, structurally and functionally diverse cilia. *Trends Cell Biol.* 19, 306–316.
- Starich, T.A., Herman, R.K., Kari, C.K., Yeh, W.H., Schackwitz, W.S., Schuyler, M.W., Collet, J., Thomas, J.H., Riddle, D.L., 1995. Mutations affecting the chemosensory neurons of *Caenorhabditis elegans*. *Genetics* 139, 171–188.
- Sulston, J.E., Schierenberg, E., White, J.G., Thomson, J.N., 1983. The embryonic cell lineage of the nematode *Caenorhabditis elegans*. *Dev. Biol.* 100, 64–119.
- Swoboda, P., Adler, H.T., Thomas, J.H., 2000. The RFX-type transcription factor DAF-19 regulates sensory neuron cilium formation in *C. elegans*. *Mol. Cell* 5, 411–421.
- Tabin, C.J., Vogan, K.J., 2003. A two-cilia model for vertebrate left-right axis specification. *Genes Dev.* 17, 1–6.
- Tusher, V.G., Tibshirani, R., Chu, G., 2001. Significance analysis of microarrays applied to the ionizing radiation response. *Proc. Natl. Acad. Sci. U.S.A.* 98, 5116–5121.
- Vandesompele, J., De Preter, K., Pattyn, F., Poppe, B., Van Roy, N., De Paepe, A., Speleman, F., 2002. Accurate normalization of real-time quantitative RT-PCR data by geometric averaging of multiple internal control genes. *Genome Biol.* 3 RESEARCH0034.
- Ward, S., Thomson, N., White, J.G., Brenner, S., 1975. Electron microscopical reconstruction of the anterior sensory anatomy of the nematode *Caenorhabditis elegans*. *J. Comp. Neurol.* 160, 313–337.
- Williams, C.L., Li, C., Kida, K., Inglis, P.N., Mohan, S., Semenc, L., Bialas, N.J., Stupay, R.M., Chen, N., Blacque, O.E., Yoder, B.K., Leroux, M.R., 2011. MKS and NPHP modules cooperate to establish basal body/transition zone membrane associations and ciliary gate function during ciliogenesis. *J. Cell Biol.* 192, 1023–1041.
- Williams, C.L., Masyukova, S.V., Yoder, B.K., 2010. Normal ciliogenesis requires synergy between the cystic kidney disease genes MKS-3 and NPHP-4. *J. Am. Soc. Nephrol.* 21, 782–793.
- Williams, C.L., Winkelbauer, M.E., Schafer, J.C., Michaud, E.J., Yoder, B.K., 2008. Functional redundancy of the B9 proteins and nephrocystins in *Caenorhabditis elegans* ciliogenesis. *Mol. Biol. Cell* 19, 2154–2168.
- Winkelbauer, M.E., Schafer, J.C., Haycraft, C.J., Swoboda, P., Yoder, B.K., 2005. The *C. elegans* homologs of nephrocystin-1 and nephrocystin-4 are cilia transition zone proteins involved in chemosensory perception. *J. Cell Sci.* 118, 5575–5587.
- Wolfgram, U., Schmitt, A., 2000. Rhodopsin transport in the membrane of the connecting cilium of mammalian photoreceptor cells. *Cell Motil. Cytoskeleton* 46, 95–107.
- Wong, S.Y., Seol, A.D., So, P.L., Ermilov, A.N., Bichakjian, C.K., Epstein Jr., E.H., Dlugosz, A.A., Reiter, J.F., 2009. Primary cilia can both mediate and suppress Hedgehog pathway-dependent tumorigenesis. *Nat. Med.* 15, 1055–1061.
- Zaghloul, N.A., Katsanis, N., 2009. Mechanistic insights into Bardet-Biedl syndrome, a model ciliopathy. *J. Clin. Invest.* 119, 428–437.

Supplemental Figure 1

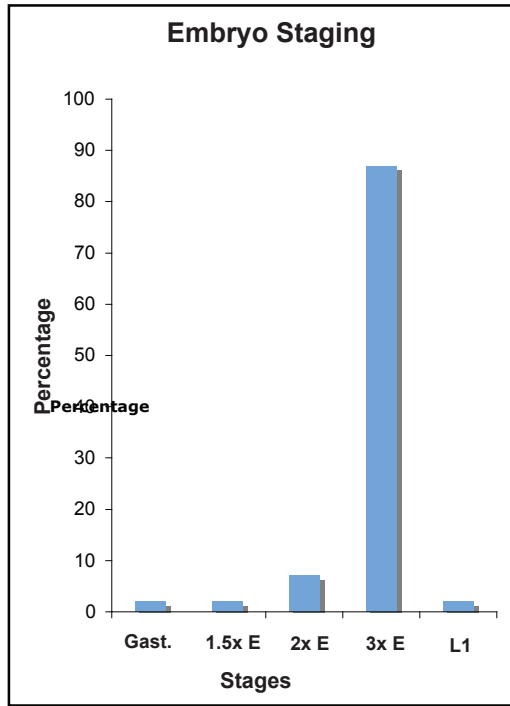
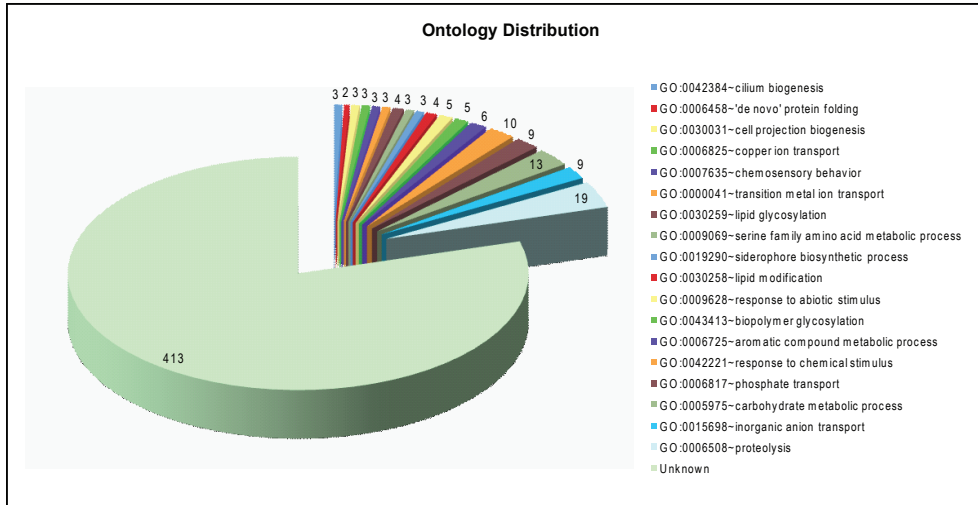


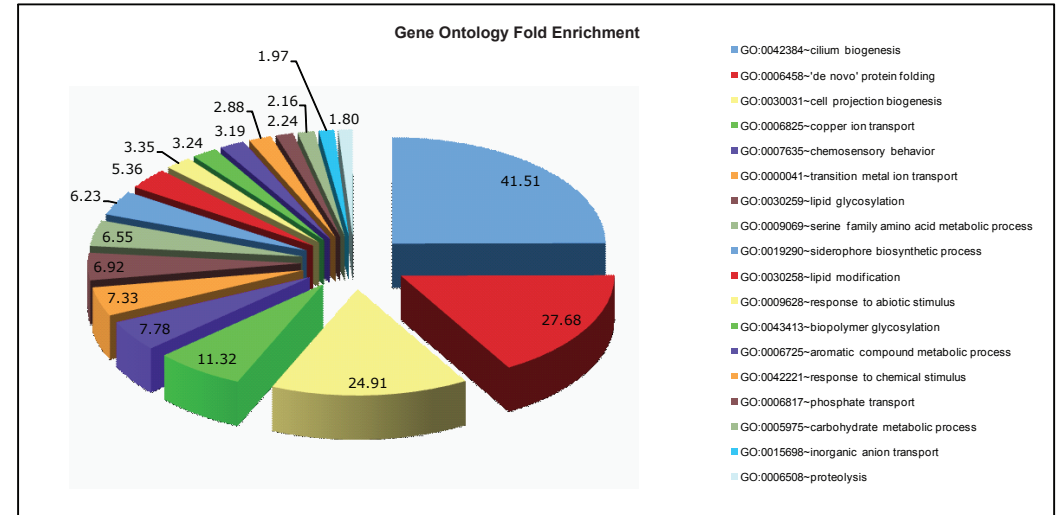
Figure Legend (X - axis)

- Gast. - Upto gastrulation stage embryos
- 1.5x E - Comma and 1.5-fold stage embryos
- 2x E - 2-fold stage embryos
- 3x E - 3-fold stage embryos
- L1 - L1 larvae

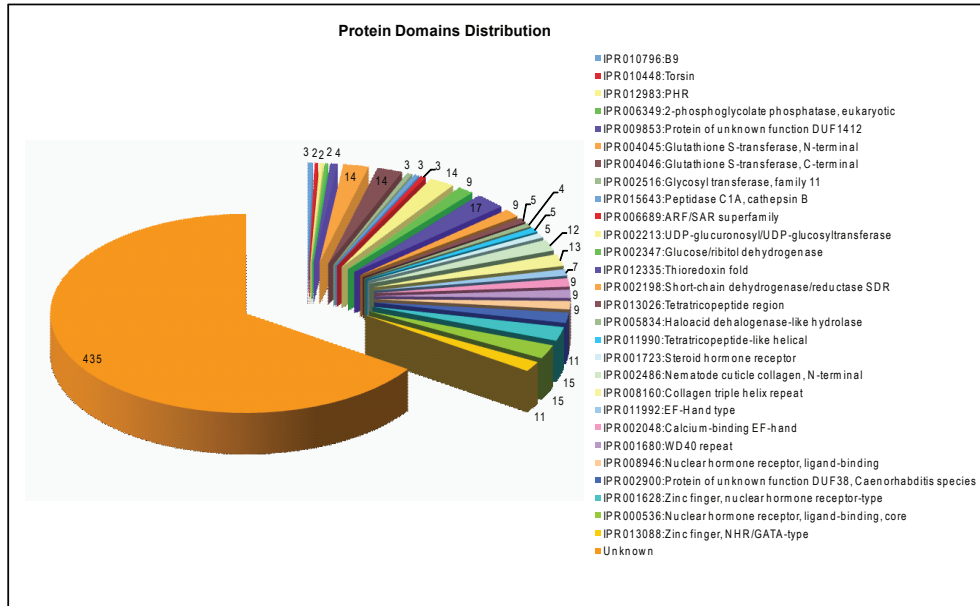
Supplemental Figure 2



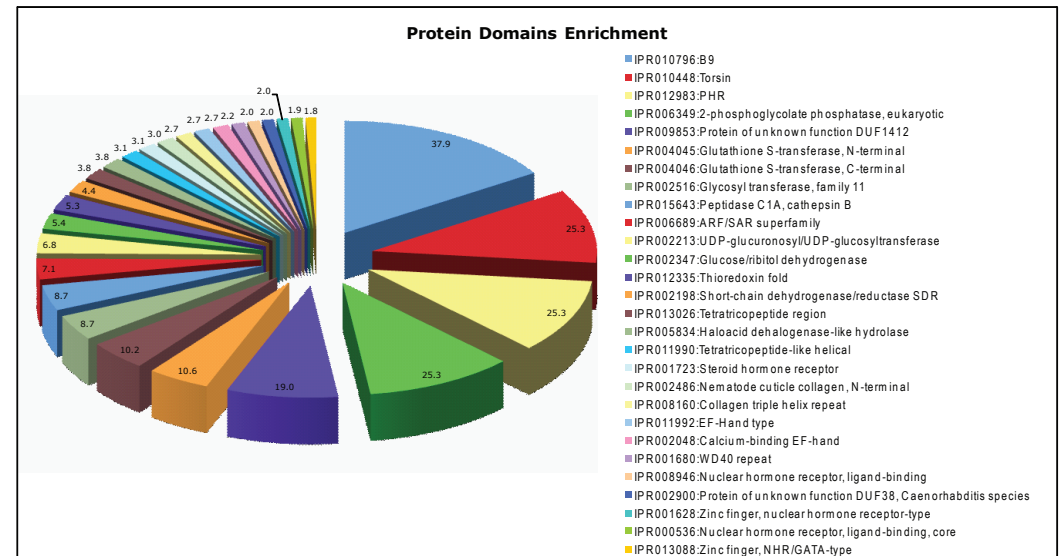
Supplemental Figure 2a: Gene Ontology distribution among the downregulated genes using Class Comparison.



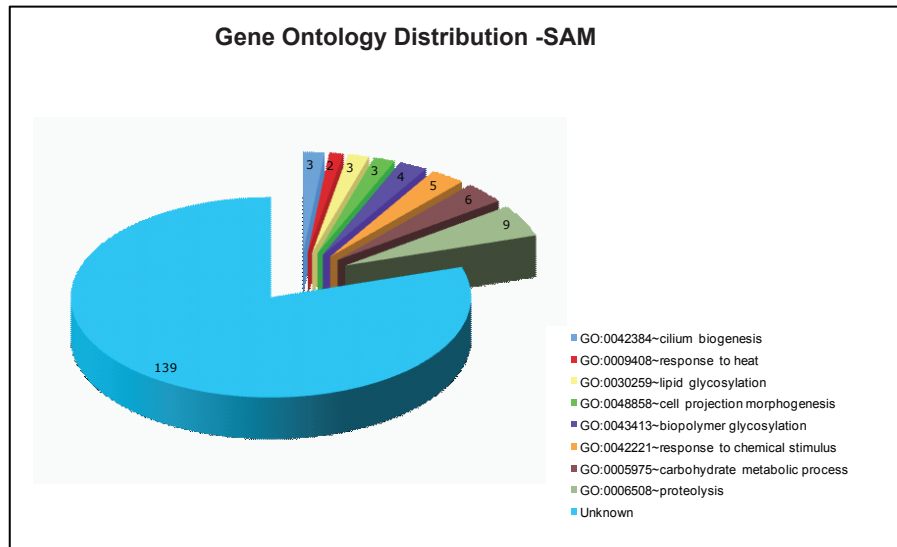
Supplemental Figure 2b: Gene Ontology enrichment among the downregulated genes using Class Comparison.



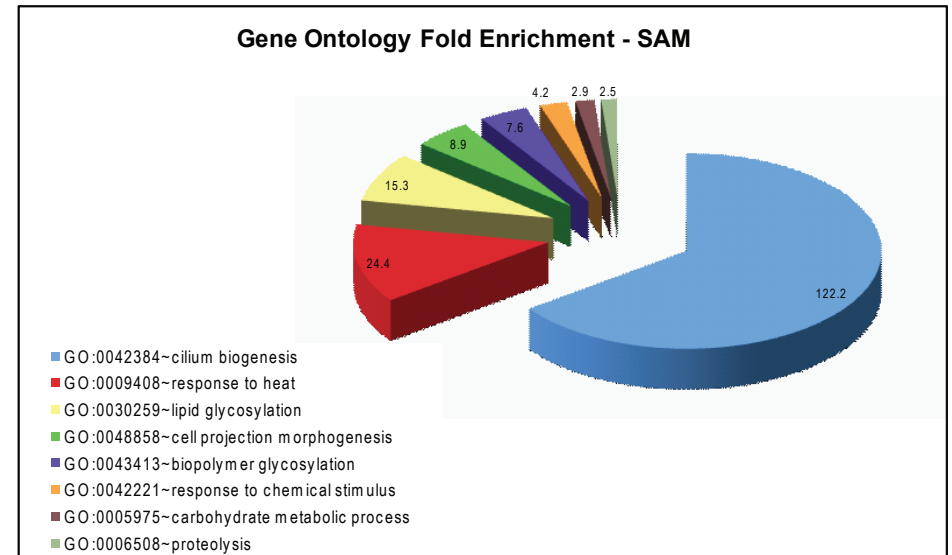
Supplemental Figure 2c: Protein domains distribution among the downregulated genes using Class Comparison.



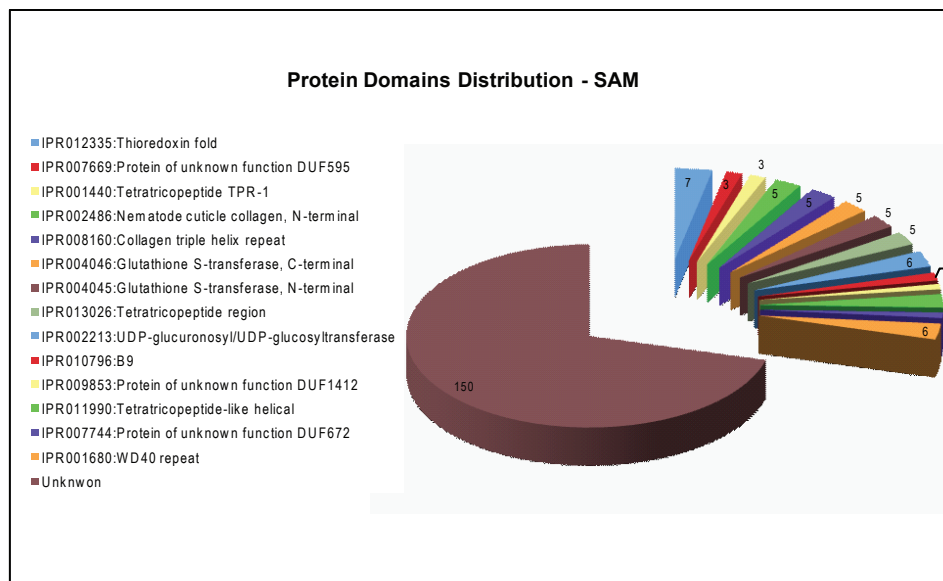
Supplemental Figure 2d: Protein domains enrichment among the downregulated genes using Class Comparison.



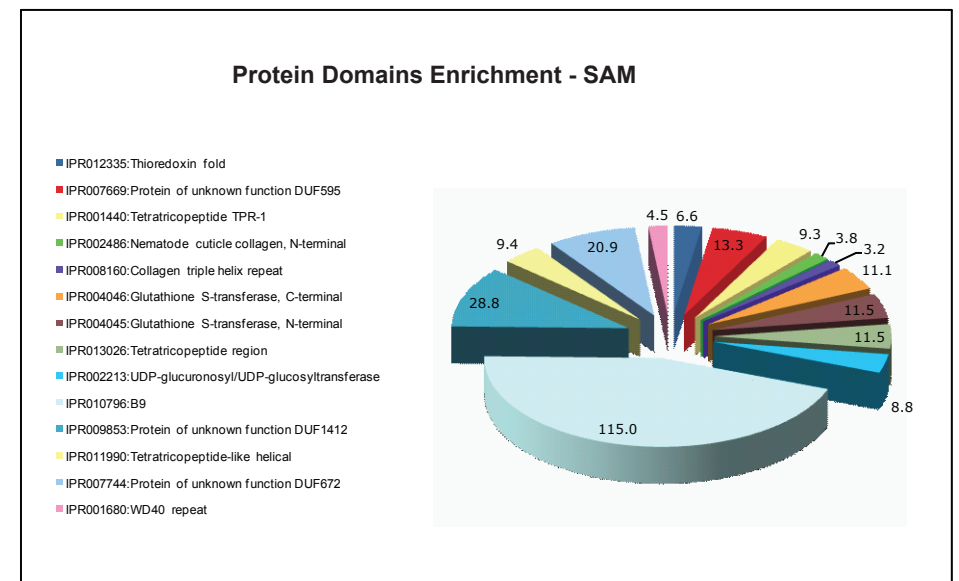
Supplemental Figure 2e: Gene Ontology distribution among the downregulated genes using SAM.



Supplemental Figure 2f: Gene Ontology enrichment among the downregulated genes using SAM.



Supplemental Figure 2g: Protein domains distribution among the downregulated genes using SAM.



Supplemental Figure 2h: Protein domains enrichment among the downregulated genes using SAM.

Supplemental Figure 3

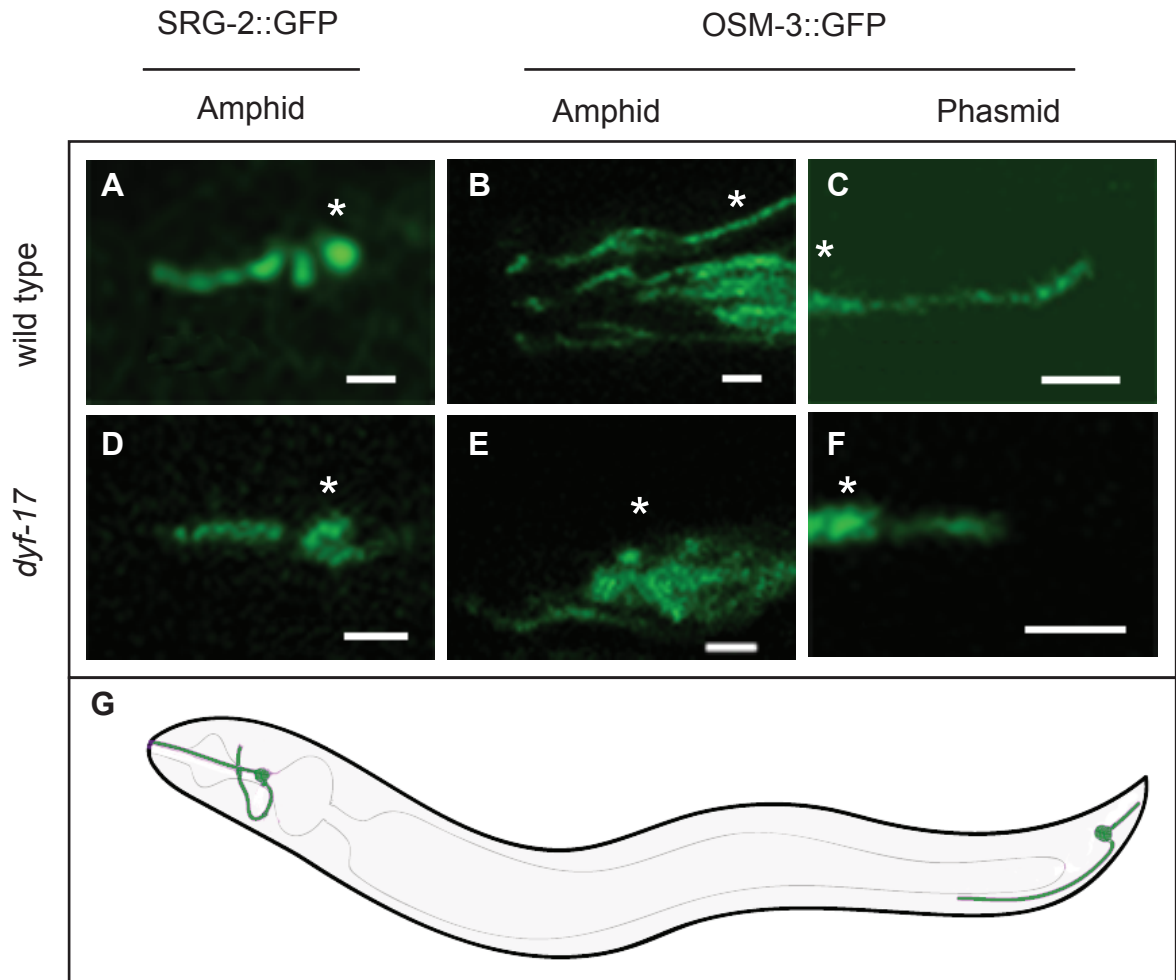


Table S1 – *C. elegans* strains and transgenes used in this study.

A. Strains

Strain	Genotype
CB3323	<i>che-13(e1805) I</i>
CX3344	<i>lin-15(n765ts) kyls53 X</i>
EG175	<i>dyf-17(ox175) V</i>
ET100	<i>dyf-18(ok200) IV</i> (6x outcrossed)
JT204	<i>daf-12(sa204) X</i>
JT5010	wild type N2 Bristol
JT6924	<i>daf-19(m86) II; daf-12(sa204) X</i>
MT3559	<i>dyf-9(n1513) V</i>
MX60	<i>myEx10</i>
MX254	<i>nxEx [kap-1]</i>
MX255	<i>ejEx1</i>
MX316	<i>nxEx [che-2]</i>
MX467	<i>dyf-18 IV; yhEx2</i>
MX468	<i>dyf-18 IV; nxEx [che-2]</i>
MX469	<i>dyf-18 IV; myEx10</i>
MX471	<i>dyf-18 IV; nxEx [kap-1]</i>
MX497	<i>dyf-18 IV; ejEx1</i>
OE3146	<i>daf-12(sa204) X; ofEx114</i>
OE3661	<i>dyf-17(ox175) V; ofEx461</i>
OE3663	<i>dyf-17(ox175) V</i> (2x outcrossed)
OE4013	<i>dyf-17(ox175) V</i> (4x outcrossed)
OE4101	<i>dyf-17(ox175) V; ofEx742</i>
OE4105	<i>dyf-17(ox175) V; ofEx746</i>
OE4106	<i>dyf-17(ox175) V; kyls141</i>
OE4107	<i>dyf-17(ox175) V; myls1</i>
OE4108	<i>dyf-17(ox175) V; kyls53</i>
OE4116	<i>ncl-1(e1865) unc-36(e251) III; osm-6(p811) V; mnIs17; ofEx779</i>
OE4118	<i>dyf-17(ox175) V; kyEx123</i>
OE4119	<i>dyf-17(ox175) V; kyEx162</i>
PR813	<i>osm-5(p813) V</i>
SP2101	<i>ncl-1(e1865) unc-36(e251) III; osm-6(p811) V; mnIs17</i>
YH2	<i>yhEx2</i>

B. Transgenes (extrachromosomal arrays and integrated transgenes)

Transgene	Genotype
<i>ejEx1</i>	<i>osm-3p::osm-3::gfp; rol-6(su1006)</i>
<i>kyEx123</i>	<i>tax-2p::tax-2::gfp; lin-15(+)</i>
<i>kyEx162</i>	<i>srg-2p::srg-2::gfp; lin-15(+)</i>
<i>kyls53</i>	<i>odr-10p::odr-10::gfp; lin-15(+)</i>
<i>kyls141</i>	<i>osm-9p::osm-9::gfp; lin-15(+)</i>
<i>mnIs17</i>	<i>osm-6p::osm-6::gfp; unc-36(+)</i>
<i>myEx10</i>	<i>che-11p::che-11::gfp; rol-6(su1006)</i>
<i>myls1</i>	<i>pkd-2p::pkd-2::gfp; cc::GFP</i>
<i>nxEx</i>	<i>che-2p::che-2::gfp; rol-6(su1006)</i>
<i>nxEx</i>	<i>kap-1p::kap-1::gfp; rol-6(su1006)</i>
<i>ofEx114</i>	<i>bbs-7p::gfp; rol-6(su1006)</i>
<i>ofEx461</i>	<i>bbs-7p::gfp; elt-2p::mCherry</i>
<i>ofEx742</i>	<i>dyf-17p::dyf-17::gfp; che-13p::mCherry; elt-2p::mCherry</i>
<i>ofEx746</i>	<i>dyf-17p::dyf-17::gfp; elt-2p::mCherry</i>
<i>ofEx779</i>	<i>dyf-17p::dyf-17::mCherry; elt-2p::mCherry</i>
<i>yhEx2</i>	<i>osm-5p::osm-5::gfp; rol-6(su1006)</i>